Monthly Notices
of the
ROYAL ASTRONOMICAL SOCIETY

MNRAS **486,** 4590–4611 (2019)
Advance Access publication 2019 April 18

doi:10.1093/mnras/stz1019

Determining the recurrence time-scale of long-lasting YSO outbursts

Carlos Contreras Peña,★ Tim Naylor and Sam Morrell
School of Physics, Astrophysics Group, University of Exeter, Stocker Road, Exeter EX4 4QL, UK

Accepted 2019 April 5. Received 2019 April 5; in original form 2019 January 23

ABSTRACT

We have determined the rate of large accretion events in Class I and II young stellar objects (YSOs) by comparing the all-sky digitized photographic plate surveys provided by SuperCOSMOS with the latest data release from *Gaia* (DR2). The long mean baseline of 55 yr along with a large sample of Class II YSOs (≃15 000) allows us to study approximately 1 million YSO-years. We find 139 objects with $\Delta R \geq 1$ mag, most of which are found at amplitudes between 1 and 3 mag. The majority of YSOs in this group show irregular variability or long-lasting fading events, which is best explained as hotspots due to accretion or by variable extinction. There is a tail of YSOs at $\Delta R \geq 3$ mag and they seem to represent a different population. Surprisingly many objects in this group show high-amplitude irregular variability over time-scales shorter than 10 yr, in contrast with the view that high-amplitude objects always have long outbursts. However, we find six objects that are consistent with undergoing large, long-lasting accretion events, three of them previously unknown. This yields an outburst recurrence time-scale of 112 kyr, with a 68 per cent confidence interval [74–180] kyr. This represents the first robust determination of the outburst rate in Class II YSOs and shows that YSOs in their planet-forming stage do in fact undergo large accretion events, and with time-scales of ≃100 000 yr. In addition, we find that outbursts in the Class II stage are ≃10 times less frequent than during the Class I stage.

Key words: stars: formation – stars: pre-main-sequence – stars: protostars – stars: variables: T Tauri, Herbig Ae/Be.

1 INTRODUCTION

The crucial period for planet formation is between ≃1 Myr (when the first planetesimals in our own Solar system were formed Pfalzner et al. 2015), and ≃10 Myr when the protoplanetary discs around most stars have dissipated (e.g. Bell et al. 2013). This corresponds exactly to the Class II phase of young stellar evolution (see e.g. Dunham et al. 2014, for a definition of the stages of young stellar evolution). Therefore properties of the disc, such as surface density or temperature, play a key role in the formation and evolution of protoplanets. These properties determine, for example, the outer boundary condition for the gas accretion rate of the protoplanets, enter into migration rates or determine the location of the snowline, the latter having an impact on the surface density of solids (see e.g. Mordasini et al. 2015).

The aforementioned disc characteristics depend on the accretion rate from the disc on to the central star. Theoretical models show that accretion on to the central star is unlikely to be a steady process (see e.g. Vorobyov & Basu 2015), with observational support arising from the analysis of knots along jets from young stars (e.g. Makin & Froebrich 2018) as well as outbursts in YSOs (e.g. Hartmann & Kenyon 1996). However, planet formation models fail to include this effect and generally assume that the accretion rate decreases steadily with time (e.g. Mulders, Pascucci & Apai 2015), with some models including a dependence with the mass of the central star (Kennedy & Kenyon 2008).

The changes in the accretion rate through circumstellar discs (if they occur) could have a profound effect on the emerging planetary systems. For example, Hubbard (2017b) argues that large accretion events can help to solve the so-called meter barrier problem (Boley, Morris & Ford 2014) and allow the *in situ* formation of rocky planets even at distances of ≃1.5 au. It also helps to explain the small size of Mars (Chambers 2014). These events can also promote the formation of Jupiter- and Saturn-like gas giants (Hubbard 2017a). Finally, the increase of the central luminosity due to changes of the accretion rate (as small as a factor of two) will drive the snow lines for various ices (used to predict the composition of planets) towards larger radii (Garaud & Lin 2007). This effect has already been observed in the known eruptive young stellar object (YSO) V883 Ori, where the water snow line is found at a distance of 42 AU from the central star, far beyond the expected location for a 1 $M_\odot$ star (Cieza et al. 2016). The observations of calcium–aluminium-rich inclusions in chondrites (Wurm & Haack

★ E-mail: cecontrep@gmail.com

2009) and the depletion of lithophile elements in Earth (Hubbard & Ebel 2014) could be evidence for large eruptions in our own Solar system.

Variable accretion in YSOs can be caused by a variety of different physical mechanisms and there may exist a continuum of outbursting behaviour with a range of amplitudes and time-scales (Cody et al. 2017). Stochastic accretion bursts in an instability-driven accretion regime lead to changes in the accretion rate up to 700 per cent over 1-10 d (e.g. Venuti et al. 2014; Cody et al. 2017). Large changes of accretion rate, increasing from typical rates of 10^{-7} up to 10^{-4} $M_{\odot}$ yr^{-1}, with outburst durations of weeks to 100 yr, which can increase the central luminosity to $100\,L_{\odot}$ (e.g. Hartmann & Kenyon 1996), are observed in eruptive YSOs (the FUors, EXors, and MNors, e.g. Audard et al. 2014; Contreras Peña et al. 2017b). Here, some kind of disc instability, such as gravitational instabilities (GIs, Vorobyov & Basu 2005, 2006) or planet-induced thermal instabilities (e.g. Lodato & Clarke 2004), are suggested as explanations of the large variability.

However, many aspects of the so-called eruptive YSOs are still uncertain. The frequency and amplitude of the outbursts is not well constrained (e.g. Scholz, Froebrich & Wood 2013). In addition, there is controversy as to whether the very largest outbursts are associated with the Class II planet building phase at all, or are just limited to the pre-planet-forming (Class 0/I) phase (cf. Sandell & Weintraub 2001, with Miller et al. 2011).

In this paper, we present the results of the study we conducted using *Gaia* and the Schmidt photographic plate surveys for a large sample of YSOs. It is our aim to answer the questions of outburst amplitudes and frequencies during the planet-forming stage of young stellar evolution. This paper is divided as follows: in Section 2, we present the data used to maximize the time baseline and the sample size as well as describing how the sample was classified as Class II YSOs. In Section 3, we present an outline of our method to select high-amplitude variability and discuss the issues we found when applying the method to our sample. Section 4 presents a discussion on the distribution of amplitudes for the variability of Class II YSOs. In Section 5, we show the steps taken to select the YSOs showing long-term outbursts where variability is most likely driven by dramatic episodes of enhanced accretion. From the latter sample, in Section 6, we determine the outburst rate during the Class II stage and compare it to previous theoretical and observational estimates. In Section 7, we present a number of caveats that could affect our estimate of the outburst rate, whilst in Section 8, we discuss the implications of our result on the likely physical mechanisms driving the outburst during the Class II stage. Finally, Section 9 shows a summary of our results.

2 DATA

To establish the recurrence rate of accretion related outbursts during the planet-forming stage, it is important to maximize both the time baseline and the number of YSOs surveyed (see e.g. Hillenbrand & Findeisen 2015). In this paper, we achieve both by comparing the magnitudes of a large sample of Class II YSOs from the photographic atlases provided by the SuperCOSMOS Sky Survey (hereafter SSS, Hambly et al. 2001) with the latest *Gaia* data release (DR2).

We note that the current classification system of eruptive YSOs is a largely phenomenological one based on photometric and spectroscopic characteristics, with long-term outbursts falling into the FU Orionis (FUor) class and short-term, repetitive outbursts classified as EXors. However, the more recent data show characteristics that have been difficult to classify into the original subclasses (see e.g. Contreras Peña et al. 2017b). Given this, during the remainder of the paper, we will not ascribe a class to the dramatic accretion events that we are searching for, but we will simply use a physical classification and refer to them as high-amplitude, long-term accretion events.

2.1 Time baseline

The SSS has digitized the entire sky in three colours (*B*, *R*, and *I*), whilst providing a second epoch in *R*, by scanning Schmidt photographic plates (Hambly et al. 2001). The observations took place during the second half of the 20th century, reaching a depth of $R \simeq 20$ mag. The photographic surveys included in SuperCOSMOS are the Science and Engineering Research Council (SERC)-J/EJ (Cannon 1984), SERC-ER (Cannon 1984), Australian Astronomical Observatory (AAO)-R (Morgan et al. 1992), European Southern Observatory (ESO)-R (West 1984), the first-epoch Palomar Sky Survey (POSS-I) E (Minkowski & Abell 1963), and the second-epoch Palomar Sky Survey (POSS-II) B, R, and I (Reid et al. 1991) surveys. For a more detailed description, see table 1 of Hambly et al. (2001).

The *Gaia* mission (Gaia Collaboration et al. 2018) has provided the first all-sky photometric survey that is able to match the depth of the photographic Palomar and ESO/SERC surveys. This provides the chance of studying the long-term variability of approximately 1 billion stars with a minimum and maximum time baselines of 15 and 66 yr, respectively.

2.2 The sample

2.2.1 Initial selection

To obtain the largest possible sample, we assembled a very inclusive sample of YSOs, and then identified the Class II YSOs using their spectral energy distribution (SED).

The first step consisted of searching the SIMBAD data base (Wenger et al. 2000) for Galactic sources with classifications that make them likely to be a YSO. We included objects with classification as pre-main-sequence stars (pr∗), pre-main-sequence star candidate (pr?), emission lines star (em∗), variable star of Orion type (or∗), Herbig Ae/Be star (Ae∗), Herbig Ae/Be star candidate (Ae?), Herbig-Haro object (HH), FU Orionis star (FU∗), T Tauri-type star (TT∗), T Taur-type star candidate (TT?), YSO (Y∗O), and YSO candidate (Y∗?). The search yielded 77 873 objects.

The SIMBAD classification does not indicate the likely evolutionary stage of the objects in our sample. The observed SED of YSOs between $2 < \lambda < 20$ μm is generally used to determine the likely evolutionary stage of the system (e.g. Lada 1987; Greene et al. 1994; Dunham et al. 2014). Objects where the infalling envelope has dissipated, but the star is still accreting material from a circumstellar disc, are known as Class II YSOs, and it is during this stage where planet formation is believed to occur (see Introduction). Therefore, we had to determine the fraction of our sample that show colours and SEDs consistent with those of Class II YSOs.

2.2.2 Classification

We crossmatched our sample ($r < 1$ arcsec) with several studies that provide a class for YSOs in known star formation regions[1] (Evans et al. 2003; Chavarría et al. 2008; Connelley, Reipurth & Tokunaga 2008; Gutermuth et al. 2008; Koenig et al. 2008; Evans et al. 2009; Gutermuth et al. 2009; Kirk et al. 2009; Billot et al. 2010; Rebull et al. 2010, 2011; Rivera-Ingraham et al. 2011; Allen et al. 2012; Megeath et al. 2012; Marton et al. 2016). All of these provide a classification based on the near- to mid-infrared (IR) SEDs of the YSOs. We found that most of the objects with a crossmatch were contained within the studies of Marton et al. (2016), Megeath et al. (2012), Evans et al. (2003) and Gutermuth et al. (2009). The Marton et al. study is based on the Wide-field Infrared Survey Explorer (*WISE*) all-sky survey and as such contains the largest number of sources. Given this, for better consistency when trying to classify our sample we gave the Marton et al. (2016) study preference over Megeath et al. (2012), Evans et al. (2003), and Gutermuth et al. (2009) as these are based on specific areas of star formation. The classification of YSOs in our sample is explained below.

*Marton et al. (**2016**)*: through the use of a supervised learning algorithm, Marton et al. (2016) classify objects as YSOs based on Two-Micron All-Sky Survey (2MASS) JHK_s (Skrutskie et al. 2006) and *WISE* (Wright et al. 2010) photometry. However, the study does not provide a direct classification as Class II YSOs, and instead yields a classification either as Class I/II or Class III YSOs. To identify the Class II YSOs, we made use of the classification criteria of Koenig & Leisawitz (2014) which are based on *WISE* bands *W*1 (3.4 μm), *W*2 (4.6 μm), and *W*3 (12 μm) bands (see Fig. 1). The latter yielded 3253 Class II YSOs. We note that Koenig & Leisawitz (2014) define different criteria to discard possible contaminant sources (active galactic nuclei, AGNs, resolved polycyclic aromatic hydrocarbon emission, among others) before attempting to classify sources in their sample as YSOs, however pre-selection using the Marton et al. catalogue has ensured our sample comprises true YSOs and as such we do not believe the criteria select contaminant objects.

*Megeath et al. (**2012**)*: this study is based on 2MASS JHK_s, IRAC (Fazio et al. 2004), and MIPS (Rieke et al. 2004) *Spitzer* photometry of the Orion A and B molecular clouds. The authors provide a value for the slope of the SED at the IRAC wavelengths (spectral index, $\alpha_{\rm IRAC}$). From the latter, 1671 YSOs show values $-1.6 < \alpha < -0.3$ (see Fig. 1); following Greene et al. (1994) these were classified as Class II YSOs. From those objects with no value of α, 605 have reliable K_s, I1 (3.6 μm), and I2 (4.5 μm) photometry as well as values for the *K*-band extinction, $A_{\rm Ks}$. We were thus able to classify them as Class II YSOs using the criteria established in appendix A of Gutermuth et al. (2009, see Fig. 1). For the remaining objects which cannot be classified through these two methods, we found 86 objects that are classified as disc objects in Megeath et al. (2012), thus we assumed that these were very likely Class II YSOs.

*Gutermuth et al. (**2009**)*: the authors provide 2MASS JHK_s, IRAC, and MIPS *Spitzer* photometry for 36 young, nearby star-forming clusters, where they also provide an evolutionary class for YSOs in these areas (see their appendix A). Based on this classification, we found 1060 Class II YSOs that were added to our list.

*Evans et al. (**2003**)*: The 'Cores to discs' (c2d) *Spitzer* legacy project provides 2MASS JHK_s, IRAC, and MIPS *Spitzer* photometry for five large and nearby molecular clouds (see e.g. Evans et al. 2009). The project also provides the slope of the SED, α, using the region between 2 and 24 μm. Using the latter information, we added 994 class II YSOs to our list.

For the objects in the SIMBAD list that were not found in any of the catalogues mentioned above, we established a likely class through the following steps.

WISE: we used the ALLWISE data release (Cutri et al. 2013). We found 4883 objects that were detected in the *W*1, *W*2, and *W*3 bands with uncertainties below 0.4[2] mag in all three bands and that can be flagged as Class II YSOs (see Fig. 1) using the criteria of Koenig & Leisawitz (2014).

2MASS: 1536 objects have reliable 2MASS photometry (quality flag 'AAA') and can be flagged as Class II YSOs based on their location in the $J - H$ versus $H - K_s$ colour–colour diagram (see Fig. 1), i.e. they show larger $H - K_s$ colours than main-sequence stars and have colours that are consistent with those of classical T Tauri stars (CTTS) as defined by the CTTS locus of Meyer, Calvet & Hillenbrand (1997).

MYStIX: many YSOs found in the Massive Young Star-Forming Complex Study in Infrared and X-ray (MYStIX, Feigelson et al. 2013) project are not part of the SIMBAD database. We found that 1400 of these were classified as being in the planet-forming stage, thus they were also added to our sample.

In summary, we were able to compile a list of 15 404 Class II YSOs.

3 *GAIA* VERSUS SUPERCOSMOS SEARCH

3.1 Outline method

To search for high-amplitude variables in our sample, we compared their *Gaia* magnitudes with those found in each individual SuperCOSMOS band. The SSS data were obtained from the merged source catalogue of SSS via a structured data language (SQL) query of the SuperCOSMOS Science Archive (SSA[3]), whilst *Gaia* magnitudes were obtained from the second data release (DR2) catalogue downloaded to a local machine. The method was as follows.

(i) For each YSO we searched for a *Gaia* and SSS counterpart, using a separation of 1.6 and 2 arcsec, respectively. If the YSO was not found in *Gaia*, then we set the magnitude of the object to be $G = 21$ to account for the possibility that the star was fainter than the *Gaia* limit at the time of observations. Whenever the YSO was not detected in an SSS band, we set the magnitude of the YSO to be that of the faintest SSS source with a stellar profile (class 2) in a $2^\circ \times 2^\circ$ box around the YSO in the corresponding band.

(ii) We crossmatched *Gaia* and SSS sources found in a $2^\circ \times 2^\circ$ box around each YSO, where SSS detections with stellar classification were selected. This allowed us to determine the relation between the *Gaia G* broad-band magnitude and the *B*, *R*1, *R*2, and *I* magnitudes obtained from SSS.

[1]We note that we did not attempt to search for every existing catalogue that provides a YSO classification. However, using these catalogues we were still able to create a large sample of Class II YSOs.

[2]We note that Koenig & Leisawitz (2014) require $\sigma < 0.2$ in al three bands, however we used a less strict criterion in order to include more objects in our classification.

[3]http://ssa.roe.ac.uk/

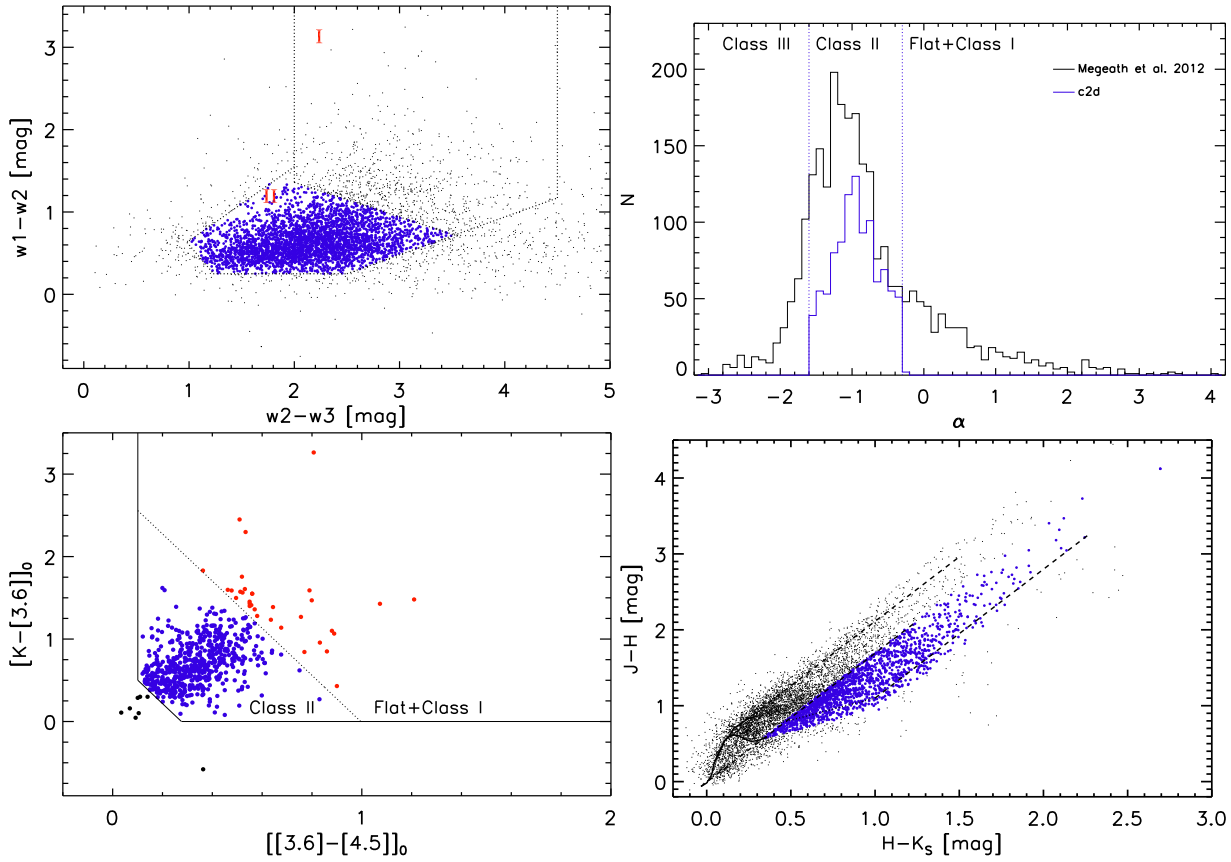

Figure 1. Examples of the different methods used to classify YSOs into the different classes of young stellar evolution. Top left: $w1 - w2$ versus $w2 - w3$ colour–colour plot for objects found in the Marton et al. (2016) catalogue (small black dots). The dotted lines mark the regions for Class I and II YSOs according to the Koenig & Leisawitz (2014) criteria. In the figure, we mark objects that fall in the Class II regions with blue circles. Top right: YSOs found in Megeath et al. (2012, solid black line) which are classified based on the spectral index determined from *Spitzer* photometry. In addition, the distribution of c2d Class II YSOs determined from α is shown in the solid blue line. The values that limit the class definitions are shown in blue dotted lines. Bottom left: YSOs found in Megeath et al. (2012) for which no value of α is published but possess reliable K_s, I1, and I2 photometry (see the main text). In the plot, Class I YSOs are shown with red circles, Class II YSOs in blue circles, and unclassified objects are marked with black circles. Bottom right: $J - H$ versus $H - K_s$ colour–colour diagram for sources that lack other forms of classification and that have reliable 2MASS photometry. Class II YSOs are marked in blue circles.

(iii) For each SSS band (whose corresponding magnitude we will call M_{sss}), we determined $G - M_{sss}$, for all objects with *Gaia* magnitudes that were found within $|G - G_{YSO}| \leq 0.2$, where G_{YSO} is the *Gaia* magnitude of the YSO being analysed. The mean value of the $G - M_{sss}$ distribution gave us the expected difference between *Gaia* and SSS for (what we assume are largely) non-variable stellar sources in the region around the YSO. A large difference between the observed $G - M_{sss}$ colour of the YSO versus the expected $G - M_{sss}$ colour estimated from non-variable sources, gave us an indication as to whether the YSO had shown any variability between the photographic surveys and *Gaia* DR2.

We quantified the variability of the YSO by treating the $G - M_{sss}$ distribution as a 4D multivariate normal distribution. We define an statistic for the variability of the source, Δ_{YSO}, as

$$\Delta_{YSO} = (\boldsymbol{x} - \boldsymbol{u})^T \boldsymbol{\Sigma}^{-1} (\boldsymbol{x} - \boldsymbol{u}) - \chi^2(5\sigma)_{k=4}, \quad (1)$$

with $\boldsymbol{x}$ the vector of the observed $G - M_{sss}$ colours for the YSO, $\boldsymbol{u}$ the vector of expected $G - M_{sss}$ colours estimated for non-variable stars, Σ is the covariance matrix determined from the expected $G - M_{sss}$ colours, and $\chi^2(5\sigma)_{k=4}$ is the value of the χ^2 distribution with 4 degrees of freedom, and for a confidence interval of 99.99996 per cent or 5σ.

To illustrate the type of objects we were looking for, we analysed the known eruptive YSOs that were part of the *Gaia* alerts sample, V2492 Cyg (e.g. Hillenbrand et al. 2013), V350 Cep (Magakian, Movsesian & Hovhannesian 1999), and ASASSN13-db (Sicilia-Aguilar et al. 2017). Fig. 2 shows a 2D representation of our method applied to the eruptive Class I YSO V2492 Cyg, where it can be seen that the observed $G - R1$ versus $G - R2$ colours of the object are located well beyond the 5σ confidence intervals. In Fig. 3, we show that the YSO is not detected in the first epoch of R (observations on 1952 September), is faint at the second epoch (observations on 1989 July) with $R = 19.8$ mag and is bright during *Gaia* observations ($G \simeq 15$ mag). We find similar results for V350 Cep and ASASSN13-db.

3.2 Finding a suitable Δ_{YSO}

We began by classifying the YSO as a variable star candidate if it satisfied the following condition

$$\Delta_{YSO} > 0, \quad (2)$$

which ensures the selection of high-amplitude variable stars.

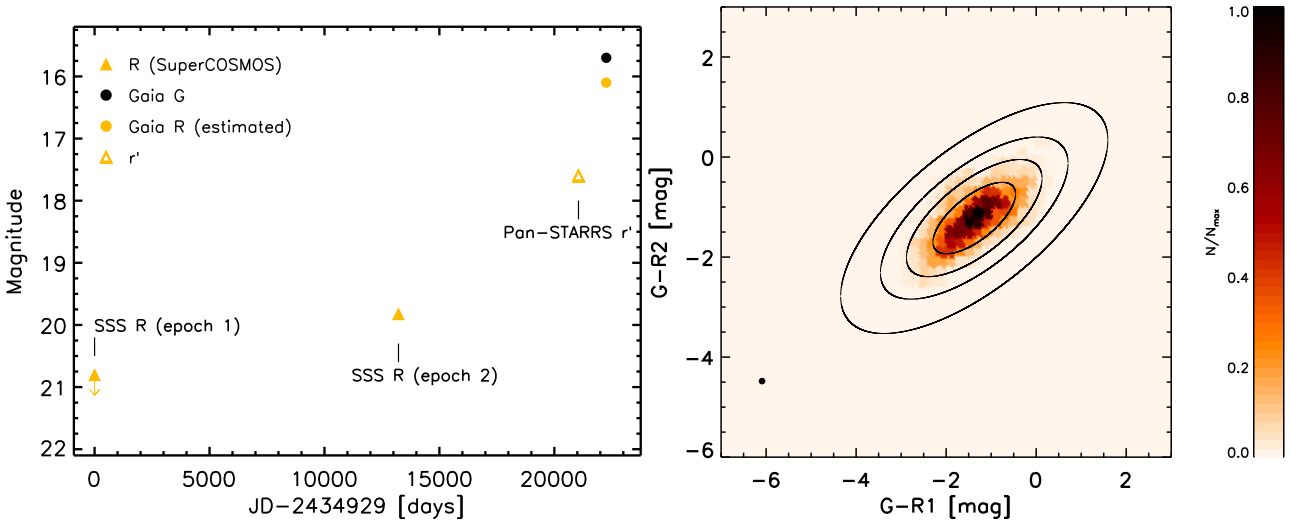

Figure 2. Left: light curve of V2492 Cyg including information from SuperCOSMOS, Pan-STARRS, and the latest magnitude provided by *Gaia*. In the plot, we mark the approximate epoch of each survey for which we present images in Fig. 3. Right: $G - R$ (second epoch) versus $G - R$ (first epoch) distribution for objects found in a $2 \times 2^{\circ}$ box around V2492 Cyg. 1σ, 2σ, 4σ, and 5σ confidence intervals are shown as thick black lines. The location of V2492 Cyg is shown as a black circle.

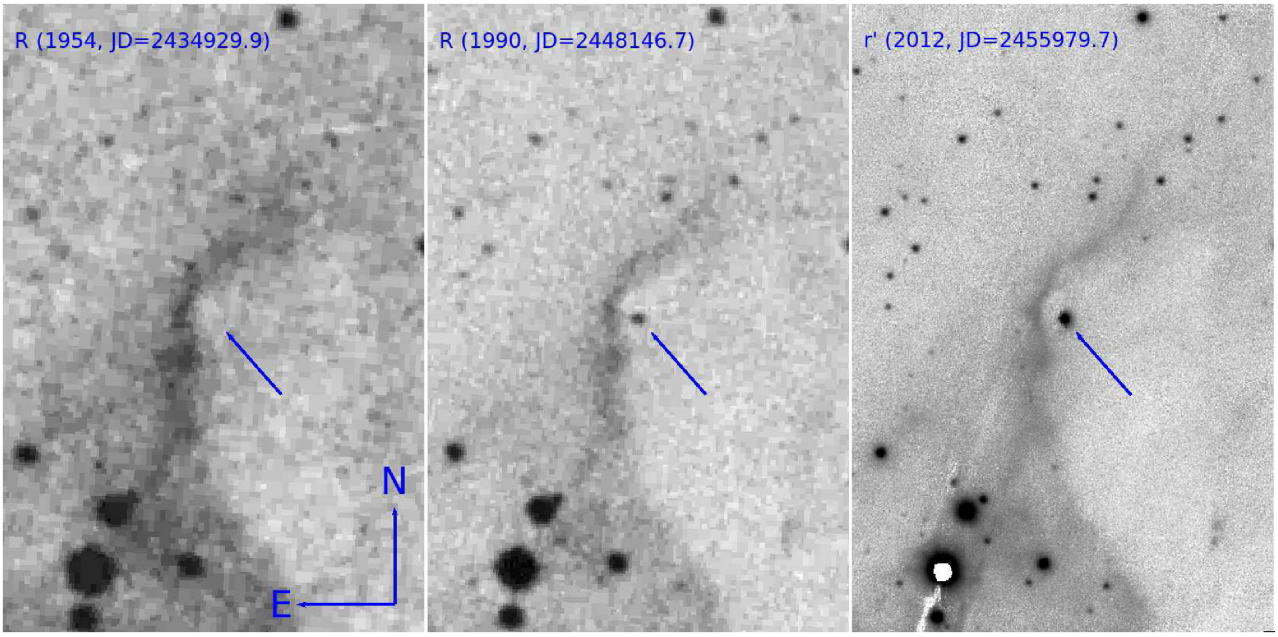

Figure 3. SuperCOSMOS POSS-I E (1954) and POSS-II R (1990) *R* plate images, and Pan-STARRS r' (2012) image for the known eruptive variable V2492 Cyg. The latter images is used as a proxy of the bright *Gaia* magnitude of the YSO. In the images, the location of the object is marked by the blue arrow. The images have a size of 2.5 arcmin $\times$ 1.7 arcmin.

To understand the types of variability that we would detect with this method, we analysed a subsample of 5000 YSOs[4] as well as a sample of known variable YSOs taken from the *Gaia* Photometric Science Alerts[5] (Wyrzykowski et al. 2012) which include a number of objects that are known eruptive YSOs. We note that in both samples, the evolutionary class of the individual YSOs was not taken into account.

This analysis yielded 24 bonafide high-amplitude ($\Delta R \geq 1.5$ mag) variable stars from the SIMBAD subsample and successfully retrieved the *Gaia* YSO alerts showing high-amplitude variability with $\Delta G > 2$ mag.

We found that most variable stars from the SIMBAD and *Gaia* alerts subsamples show low-amplitude, recurrent aperiodic variability. A literature search revealed that the variability in these low-amplitude objects is caused by physical processes other than

[4]This sample is selected from some of the categories described at the beginning of Section 2. We note that these do not include the FU Orionis star class.
[5]http://gsaweb.ast.cam.ac.uk/alerts

variable accretion. The low-amplitude objects showed lower values of $\Delta_{\rm YSO}$, whilst a few of these had positive values of $\Delta_{\rm YSO}$, but with individual values of $G - M_{\rm SSS}$, when analysed separately as a univariate distribution, that were found to be below 5σ in each band.

In the cases where we suspected variability was due to large accretion events, and in the known eruptive YSOs from the *Gaia* alerts, we found that $\Delta_{\rm YSO}$ showed a value much larger than 0. In addition, the inspection of individual values of $G - M_{\rm sss}$, when analysed separately as a univariate distribution, were found to be above 5σ in at least one band.

Given the results from this early analysis, when applying our method to the Class II YSO sample, we defined a new set of conditions for an object to be included as a candidate variable star. This was done to reduce the number of objects to inspect (see below) and to try and include only the most extreme cases of variability, and thus more likely related to large and long-lasting changes in the accretion rate. The revised conditions were as follows.

(i) $\Delta_{\rm YSO} \geq 70$ and the individual values of $G - M_{\rm sss}$, when analysed separately as a univariate distribution, to be above 5σ in at least one band.

(ii) $\Delta_{\rm YSO} \geq 100$ and the individual values of $G - M_{\rm sss}$, when analysed separately as a univariate distribution, to be below 5σ in each band.

3.3 Problems with the photographic images images

Through the initial analysis of the two YSO subsets, we were able to recognize a major source of contamination in our variable star candidates list. We found that in many objects the non-detection of the source in the SSS catalogues was probably due to problems with the plate images rather than true variability of the source. These issues were most apparent in the areas with high extinction, and were more evident in the *B* and *R* SSS images. In order to define whether the variability was driven by this issue, we first queried *Gaia* DR2 and the SSA to select sources within a box size of 3 arcmin × 3 arcmin around the YSO being analysed. Then, we crossmatched both catalogues to determine the number of objects detected both in SSS and *Gaia*, $N_{\rm sss}$. In individual filters, YSOs found in problematic areas showed a low value for the ratio $N_{\rm sss}/N_{\rm Gaia}$, with $N_{\rm Gaia}$ the total number of *Gaia* sources in the 3 arcmin × 3 arcmin box. Therefore, if the individual bands driving the variability of the YSO showed $N_{\rm sss}/N_{Gaia} < 0.45$, then this object was classified as unlikely to be a variable star.

3.4 Visual inspection of variable star candidates

We next used the results from our subsamples to inform a search for high-amplitude variable stars using all the 15 404 YSOs in our sample. The method yielded 4815 objects that fulfilled the condition established by equation (2). This number reduced to 1576 objects when we imposed the conditions of Section 3.2. From the latter, 501 objects were flagged as being in the list due to the problems with photographic plates explained in Section 3.3. Thus, we were left with 1075 variable YSO candidates.

To confirm or discard its variability, each of the 1075 variable candidates was analysed individually. The analysis included the inspection of the 3 arcmin × 3 arcmin cutout images from the photographic plates provided by the SSA, as well as comparing with the more recent images (when available) provided by the Panoramic Survey Telescope and Rapid Response System (Pan-STARRS, Chambers et al. 2016) and the SkyMapper Southern Sky Survey (Wolf et al. 2018). In addition, we also searched for additional photometry from publicly available catalogues through the VizieR catalogue access tool (Ochsenbein, Bauer & Marcout 2000). The list of the individual surveys found in Vizier that were used in our analysis is given in Appendix C. This final step revealed further sources of contamination that were not considered before the cleaning of the final sample. Most of these related to problems with bright objects, crowding, or incorrect magnitudes in SSS catalogues.

Table 1. Example of the photometry obtained for each high-amplitude variable. In the tables, we present the modified Julian date of the observations (estimated from the Julian date as MJD = JD−2400000.5), the *R*- or *r*-band magnitudes and the survey from where they are obtained. In the last column, we present a note depending on whether the magnitudes are an upper limit or if these result from transforming between different filters (marked as approximate in the table). The full table is available online.

ID	MJD	Mag	Filter	Survey	Note
V4	34 270.404	21.0	*R*	SSS(R1)	Upper limit
V4	47 880.208	21.0	*R*	SSS(R2)	Upper limit
V4	49 253.445	18.5	*R*	SSS(B)	Approximate
V4	49 654.347	18.5	*R*	SSS(I)	Approximate
V4	52 953.981	17.46	*r*	IPHAS	–
V4	56 227.446	16.79	*r*	Pan-STARRS	–
V4	56 537.365	16.49	*R*	PTF	–
V4	57 204.000	16.5	*R*	*Gaia*	Approximate

After inspection of the individual candidates, we found 139 true high-amplitude variable stars. In each case, the additional photometry from other surveys allowed us to classify the objects according to their light curves. We note that this is based only on a handful of epochs, therefore in many cases our classification is uncertain and is thus followed by a ? sign. This classification aims to select those objects where variability resembles that of long time-scale outbursts. An example of the photometry obtained for each high-amplitude variable is presented in Table 1. The full light-curve data are presented as Supporting Information.

The list of 139 high-amplitude variable stars selected with our method is shown in Table 2. Column 1 shows the designation given by us. Since the objects are ordered by amplitude, and the number gives an indication of their level of variability. Columns 2 and 3 mark the right ascension and declination of the object, respectively. The SIMBAD identification and type are shown in columns 4 and 5, whilst column 6 gives the observed (*R*) amplitude taking into account only the SSS and *Gaia* epochs (after transforming the *Gaia* *G*, and SSS *B* and *I* into *R*-band magnitudes). We note that these are approximate values. In column 7, we present a classification for the behaviour of the light curve of the YSO (Section 3.4). Column 8 provides a final classification of the light curve, which is obtained either by the analysis done in this work (see Section 5) or by information found in the literature (e.g. V26 is a known UXor), whilst column 9 shows the references to such classification. In column 10, we mark whether the object is a known variable star, whilst column 11 shows whether the SSS versus *Gaia* variability relates to the known variability of the source of if our detection relates to previously unknown variability of the source. Finally, column 12 shows the source that was used to classify the YSOs as being in the Class II stage (see Section 2.2.2).

Our sample contains 66 new variable stars, which represents 48 per cent of our sample. From the known variable stars (72 objects), we find that in 17 objects the SSS versus *Gaia* variability has not been reported previously. We note that upon further inspection objects V5, V12, V24, V32, V45, and V84 are found

Table 2. The 139 high-amplitude variable stars detected in our analysis. The full table is available online.

ID	α	δ	SIMBAD ID	SIMBAD class	ΔR	LC class	Final class	Reference	Known?	SSS?	YSO class
V1	20:58:53.72	+44:15:28.3	EM* LkHA 190	FUOr	5.2	Outburst	Long-lasting (Class I)	This work (Section 5)	Y	Y	Marton
V2	20:58:17.03	+43:53:43.3	V* V2493 Cyg	FUOr	5.0	Outburst	Long-lasting (Class II)	This work (Section 5)	Y	Y	Marton
V3	20:54:07.39	+41:34:58.1	V* V1219 Cyg	Orion V*	4.7	Repetitive fadings	Deep fades	Stecklum & Linz (2013)	Y	Y	Marton
V4	02:33:53.40	+61:56:50.1	2MASS J02335340 + 6156501	YSO	4.5	Outburst	Long-lasting (Class II)	This work (Section 5)	N	N	2M_AAA
V5[a]	05:28:54.06	−06:06:06.3	V* RX Ori	Orion V*	4.5	Periodic	Non-YSO	Lee & Chen (2007)	Y	Y	WISE_slt04
V6	21:43:00.01	+66:11:27.9	V* V350 Cep	Orion V*	4.5	Outburst	Long-lasting (Class I)	This work (Section 5)	Y	Y	Marton
V7	16:11:46.00	−25:32:00.8	V* V931 Sco	Orion V*	4.4	Irregular	Periodic ($P = 215$ d)	Pojmanski (2002)	Y	Y	Marton
V8	05:10:11.00	−03:28:26.2	2MASS J05101100 − 0328262	YSO	4.0	Irregular	Short-term outburst	Sicilia-Aguilar et al. (2017)	Y	Y	WISE_slt04
V9	08:41:06.76	−40:52:17.4	2MASS J08410676 − 4052174	Em*	4.0	Outburst	Long-lasting (class II)	This work (Section 5)	Y	N	Marton
V10	22:53:33.26	+62:32:23.6	V* V733 Cep	FUOr	4.0	Outburst	Long-lasting (Class II)	This work (Section 5)	Y	Y	Marton
V11	05:37:00.10	−06:33:27.3	V* BE Ori	Em*	4.0	Repetitive outbursts?	–	–	Y	Y	Megeath_alpha
V12[a]	16:00:07.42	−41:49:48.4	2MASS J16000742 − 4149484	Candidate YSO	3.8	Irregular	Non-YSO	Frasca et al. (2017)	N	N	C2D

Note: [a] Objects not included in any subsequent analysis.

Figure 4. Top: *R*-band amplitude histogram for the high-amplitude variable stars recovered by our search. Bottom: cumulative distribution of the *R*-band amplitude, representing the percentage of objects in our sample that are found below the corresponding magnitude level.

to be more likely non-YSOs. Therefore, although these are shown in Table 2, we did not include these objects in the following analysis of variability in the class II YSOs.

4 THE DISTRIBUTION OF CLASS II AMPLITUDES

The top plot of Fig. 4 shows the histogram of the amplitudes of our high-amplitude variable stars as determined from the SSS and *Gaia* epochs. We note that in the histogram we did not include the objects that were found to be likely non-YSOs. In addition we also did not include the three long-lasting outbursting YSOs that are more likely Class I YSOs (see Section 5.4).

In the histogram, we can see that we do not detect objects with amplitudes below 1 mag. In addition, the sample appears incomplete below 2 mag.

To obtain the distribution of amplitudes for low amplitudes we used the data set of *i*-band photometry of Cep OB3b presented in Sergison et al. (in preparation). We took the objects classified as Class II on the basis of their *Spitzer* photometry (Allen et al. 2012), which are in Sergison et al. (in preparation)'s primary sample. Importantly, variability has played no part in the selection of these stars. We took one long observation from each of 2004, 2005, 2007, and 2013 as the closest analogue we could obtain to the sampling in this paper. For each star which had 'good' photometry (as defined

by Sergison et al., in preparation) for all four datapoints we then calculated a full amplitude.

To compare both samples, we needed to estimate the fraction of stars per unit amplitude (df/dA). However, given the observed amplitudes of our YSO variables, we considered the possibility that some objects in our Class II YSO sample were too faint to have been detected in *Gaia*, even if they showed large-amplitude outbursts. We found that 3712 YSOs had no *Gaia* DR2 counterparts, but this was found to be consistent with the fact that they were also faint or not detected in SSS, so they were flagged as non-variable stars.

There is no detailed selection function for *Gaia*, but the star counts turn over at about $G \simeq 20.5$ mag (Gaia Collaboration et al. 2018). Hence, objects with $G \leq 22.5$ mag showing variability with $\Delta R \geq 2$ mag should have been detected in *Gaia* DR2. To estimate an approximate G magnitude for the 3712 YSOs that are not in *Gaia* DR2, we obtained sloan-r, J, and K photometry of the YSOs by crossmatching with catalogues from Pan-STARRS, SkyMapper, the SDSS photometric catalogue (Alam et al. 2015), DENIS (Epchtein et al. 1994), 2MASS (Skrutskie et al. 2006), UKIDSS GPS (Lucas et al. 2008), and the VISTA Variable in the Via Lactea Survey (Minniti, Lucas & VVV Team 2017). Objects that were detected with $r < 24$ mag would have been detected in *Gaia* if they had shown high-amplitude variability. Objects without r-band detections, do have J, and K photometry, so we use the information from YSOs that were detected in *Gaia* DR2 to determine a relation between the $G - J$ and $J - K$ colours. The latter fit was then used to estimate an approximate value of G for the objects that are not originally detected in *Gaia* DR2.

This method showed that 1318 YSOs had approximate G-band magnitudes that were fainter than 22.5 mag, so we believe these would have not been detected even if they had shown high-amplitude variability. Thus, for the remainder of our analysis of variability, our total sample of Class II YSOs reduces to 14 086 objects.

The comparison of df/dA between our sample and that of Sergison et al. (see Fig. 5) confirms that our sample is not complete below amplitudes of 1 mag. Both samples agree remarkably well at 2 mag. The figure also shows that at $\Delta m > 3.5$ mag, the number of objects does not fall as expected from the rate of decline observed at lower amplitudes. Instead, the distribution reaches a plateaux, which could point to YSOs at these amplitudes being part of a different population of variable stars.

5 SELECTING HIGH-AMPLITUDE ACCRETION-DRIVEN VARIABILITY

We detected a large number of high-amplitude variable YSOs. The next step consisted of determining what is the physical mechanism driving these large changes.

5.1 Physical mechanism

Variability is one of the defining characteristics of pre-main-sequence stars (e.g. Joy 1945). This occurs on a broad range of time-scales and amplitudes due to various physical mechanisms. Periodic modulation of the stellar flux resulting from the rotation of cool spots in the stellar photosphere is mostly observed in weakly accreting YSOs (the so-called weak-lined T Tauri stars or WTTS) and its characterized by low level variability in the order of 0.1 mag (Herbst et al. 1994). The irregular (although sometimes periodic) variability from short-lived hotspots at the stellar surface due to accretion can reach can 2–3 mag in extreme cases (see e.g. Grankin et al. 2007). Luminosity dips caused by circumstellar dust obscuration can last days to months and with amplitudes that are effectively limitless as they depend of the optical depth of the dust obscuring the central star (see e.g Carpenter, Hillenbrand & Skrutskie 2001). Finally, changes in the accretion rate from the disc on to the central star can also cause variability, with time-scales of days to hundreds of years, in YSOs (see Introduction).

The amplitude of the variability of stars in our sample gives us an insight into the physical mechanism that drives the variability in these YSOs. We have previously discussed that at amplitudes below 2 mag the sample is incomplete. However, this is not a problem for the purposes of this study as we are interested in the most extreme cases of accretion-related variability which we expect to have amplitudes greater than this level. We would not expect to detect YSOs where variability is caused by cool spots in the stellar photosphere, as amplitudes due to this effect are not expected to reach more than a few tenths of a magnitude. In addition our sample is comprised of Class II YSOs, where this effect is not expected to dominate. The lower number of YSOs at amplitudes below 2 mag and the non-detection at below 1 mag, allows us to conclude that we are not observing variability due to cool spots.

Figs 4 and 5 also show that the number of variable YSOs drops dramatically at amplitudes larger than 3.5 mag, but there appears to be a secondary peak at around 4.5 mag, although the position of the peak is highly dependent on the choice of bin size. However the cumulative distribution shown in Fig. 4 does reveal a bump at around 4 mag. Thus, the variable YSOs with amplitudes larger than 3.5 mag could be a different population from the objects described above. Considering the photometric characteristics of known long-lasting YSO outbursts, it is at these amplitudes that we would expect to find the majority of objects that can be classified as showing long-term, accretion-driven outbursts.

5.2 Selecting long time-scale variability

The selection of objects where variability is driven by extreme, long-term changes in the accretion rate was difficult. In many cases using just the data from SSS and *Gaia* (five epochs of observations) could give a false impression that the object is an eruptive YSO. Therefore, we made use of all the available photometry (see Section 3.4) to discard or confirm a classification as long-lasting YSO outbursts. In many cases, the classification was aided by a more exhaustive literature search.

In this analysis, we found that the majority of YSOs with amplitudes between 1 and 3 mag (101 out of 108 objects) are characterized by light curves with fading events or irregular variability (i.e. going from bright to faint states repetitively across their light curves). The variability in this group is likely to be explained by hotspots due to accretion, representing extreme cases of this type of variability (see Grankin et al. 2007) or from dust obscuration, similar to the fading events observed in AA Tau (Bouvier et al. 2013) or in RW Aur (e.g. Bozhinova et al. 2016). The remaining seven YSOs (V36, V51, V53, V56, V68, V85, and V94) were classified as a potentially having long-lasting outbursts based on their light curves.

From the 28 objects with amplitudes of $\Delta R \geq 3$ mag (variable stars V1 to V4, V6 to V11, V13 to V23, and V25 to V31), seven were classified as showing long-lasting outbursts. Amongst the 28 objects we also find objects with apparent long-lasting fading events, again likely related to extinction, and objects with irregular variability. However, given the larger amplitudes, variability due to hotspots is less likely to explain this kind of variability. Instead these are

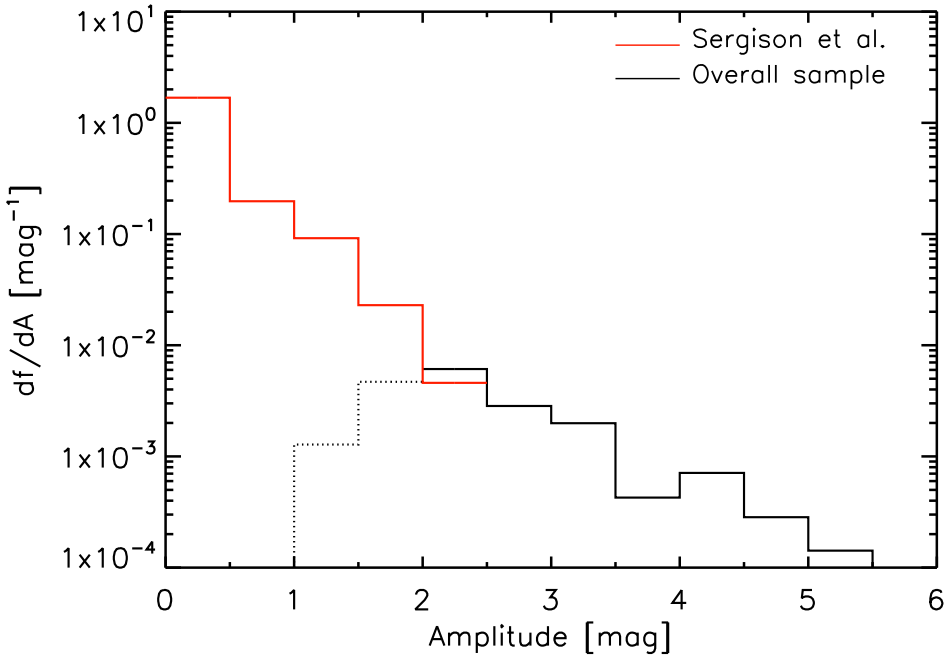

Figure 5. Fraction of stars per unit amplitude, df/dA. The solid red line shows the distribution for variable YSOs from Cep OB3b presented in Sergison et al (in preparation), whilst the solid black line marks the distribution for YSOs in this work. The dotted black line also marks the distribution of variable YSOs from this work, but for objects in the region where we are incomplete (see the main text).

more likely explained by short-term accretion events that appear as irregular given the long baseline of the light curves.

The variable star V20 (2MASS J20521294 + 4420534) illustrates the issues of classifying YSOs based only a handful of epochs. Fig. 6 shows the light curve of the source using the SSS and *Gaia* epochs, in addition we also compare the *R* and *I* images from SSS. Based only on this information, this object appears to have gone into outburst after the second epoch of *R*-band observations, becoming $\simeq$3.2 mag brighter during the I SSS observations and remaining bright until the *Gaia* observations. However, the addition of literature data and inspection of images provided by the Palomar Transient Factory (PTF, Law et al. 2009) reveals that the faint *R* magnitudes are probably part of the 'normal' variability of the source, which seems to be characterized by irregular, short-term variability (see the bottom images of Fig. 6).

A second example is V3 (V1219 Cyg), which could be easily mistaken as showing a 4.7 mag outburst between the first and second epochs of *R* SSS observations (see Fig. 7), in addition the object drives an H_2 outflow (Makin & Froebrich 2018). However, further analysis reveals that this source has been classified in the past as showing repetitive high-amplitude fading events rather than a long time-scale outburst (see Stecklum & Linz 2013).

In both examples the light curves, given only the SSS and *Gaia* data, could easily be classified as long-term outbursts. We were able to discard such classification only through the inclusion of additional data from the literature.

Therefore in trying to find objects with long-lasting outbursts, we discovered a large population of high-amplitude variable YSOs that cannot be classified as showing long-term outbursts (see Section 5.3). Changes in the accretion rate could still be the underlying cause of such variability, but objects that show repetitive and/or short-term (lasting less than $\simeq$10 yr) outbursts, such as V18 or V8 (the known short-term eruptive YSO ASASSN13-db, see Sicilia-Aguilar et al. 2017), are not included in the subsequent analysis. However, we emphasize that these are an interesting class of objects in their own right.

In addition, many objects show apparent long-lasting fading events. This type of variability is explained by obscuration of the central star by structures in the disc located at large distances and above the mid-plane of the disc (see e.g. Bouvier et al. 2013). This is interesting in the context of discs and planet formation. The migration of giant planets due to interactions with the disc (also known as type II migration, Ida & Lin 2004) can open up gaps in the disc which could lead to scale height bumps (Baruteau & Papaloizou 2013) or to a misalignment between the inner and outer discs (Lubow & Martin 2016), that could lead to fading events. We note, however, that mechanisms such as dusty outflows could also lead to these type of events (Davies et al. 2018).

Again, these objects are interesting findings, but further analysis of them is beyond the scope of this paper.

5.3 Outbursts

To determine an outburst rate from our analysis, we needed to select only objects where a classification as a long-lasting YSO outburst was very likely. In this sense YSOs where changes in the accretion rate might be the physical mechanism driving the variability, but which show repetitive and/or short-term outbursts are not included (see above). Additionally, we did not include objects where lack of data did not allow a firm classification. For example, five out of seven objects with $\Delta R \leq 3$ mag and that were classified as potentially having long-lasting outbursts, were not included in our final sample as there was not enough data that would allow to confirm such classification.

Collating literature and database information in this way allowed us to classify nine objects as being part of the eruptive YSO class showing long-lasting outbursts (the seven objects with $\Delta R \geq 3$ mag classified as having long-lasting outbursts in Section 5.2

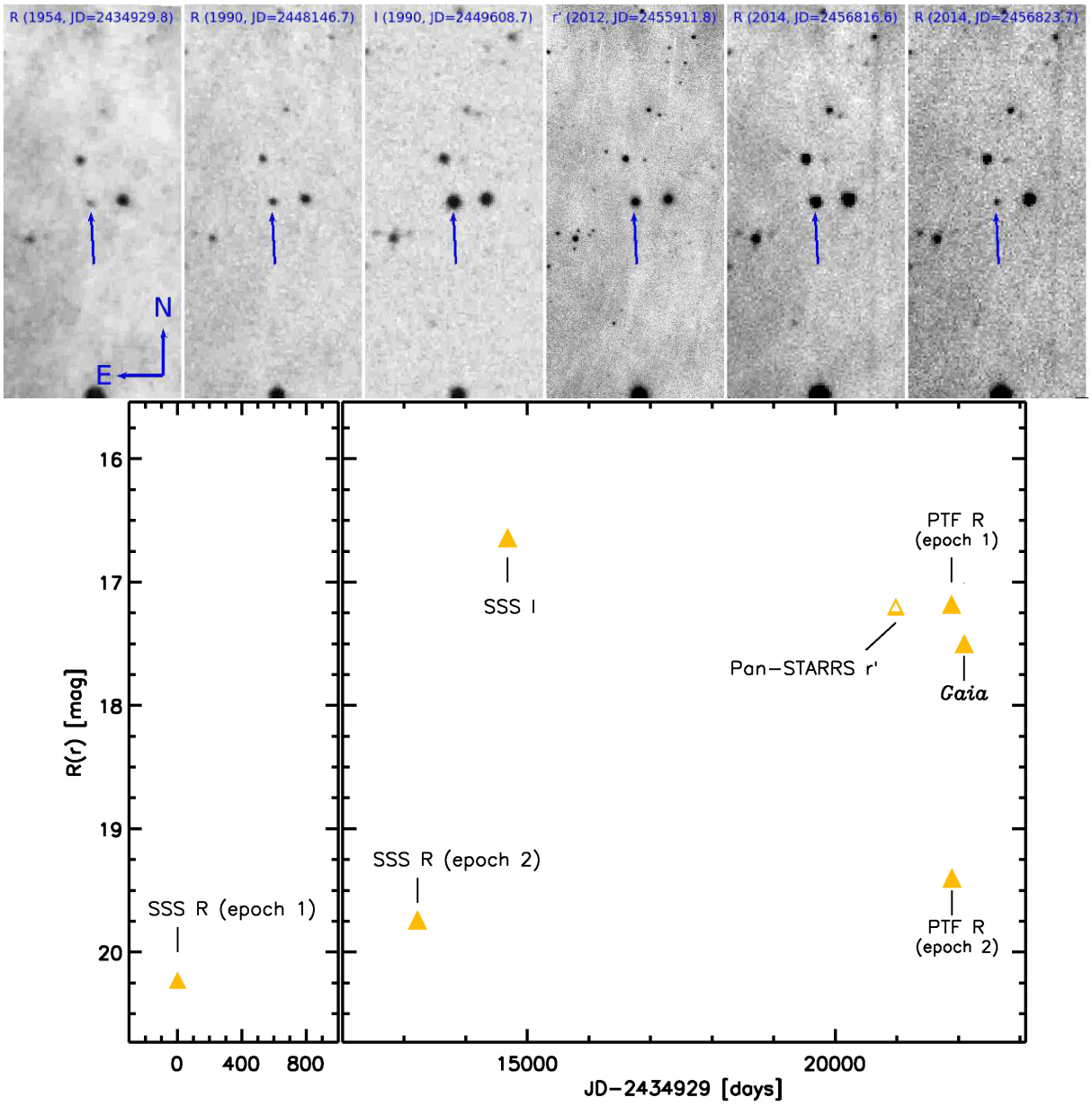

Figure 6. Top: comparison of POSS-I *R*, POSS-II *R,* and POSS-II *I* photographic plate images with sloan *r* image from Pan-STARRS (as a proxy for the *Gaia* magnitude) and *R*-band images from the PTF survey. We mark the date of observations at the top of each image, whilst the variable star is marked by a blue arrow. All of the images have a size of 3 arcmin × 1.3 arcmin. Bottom: light curve of V20 showing the *R* (filled triangles) and sloan *r* (open triangle) magnitudes. The photometry from the SSS *I* and *Gaia G* filters have been converted to approximate *R*-band magnitudes to help the clarity of the light curve. In the plot, we mark the approximate epoch of the photometry for which we present images in the top plot of the figure.

and two objects with $\Delta R < 3$ mag, V36 and V51). These include six known eruptive YSOs, V1 (LkHA 190, most commonly known as V1057 Cyg, e.g. Hartmann & Kenyon 1987), V2 (V2493 Cyg, most commonly known as HBC722, Semkov et al. 2010), V6 (V350 Cep, Ibryamov, Semkov & Peneva 2014), V10 (V733 Cep, Reipurth et al. 2007), V31 (UCAC2 30330609, most commonly known as V960 Mon, Hillenbrand 2014), and V36 (V582 Aur, Ábrahám et al. 2018). There are three previously unknown eruptive YSOs, V4 (2MASS J02335340 + 6156501), V9 (2MASS J08410676 − 4052174), and V51 (WRAY 15−488). A more extensive explanation for the classification of the previously unknown objects is presented as individual notes in Appendix A.

5.4 Class I contamination

Due to the effects of geometry, reddening or disc inclination there might not be a direct correlation between the YSO class and its evolutionary stage (see e.g. Robitaille et al. 2006). The classification of objects in Section 2.2.2 was done using near- to mid-IR data, which lead to a classification as Class II YSOs, however, longer wavelengths could reveal the presence of envelopes (see also Section 7.3 for further discussions on the contamination from Class I YSOs).

Therefore, before we determined the outburst rate from our selected YSOs, we took into consideration the possible contamination from YSOs at earlier evolutionary stages in our sample (Class I or

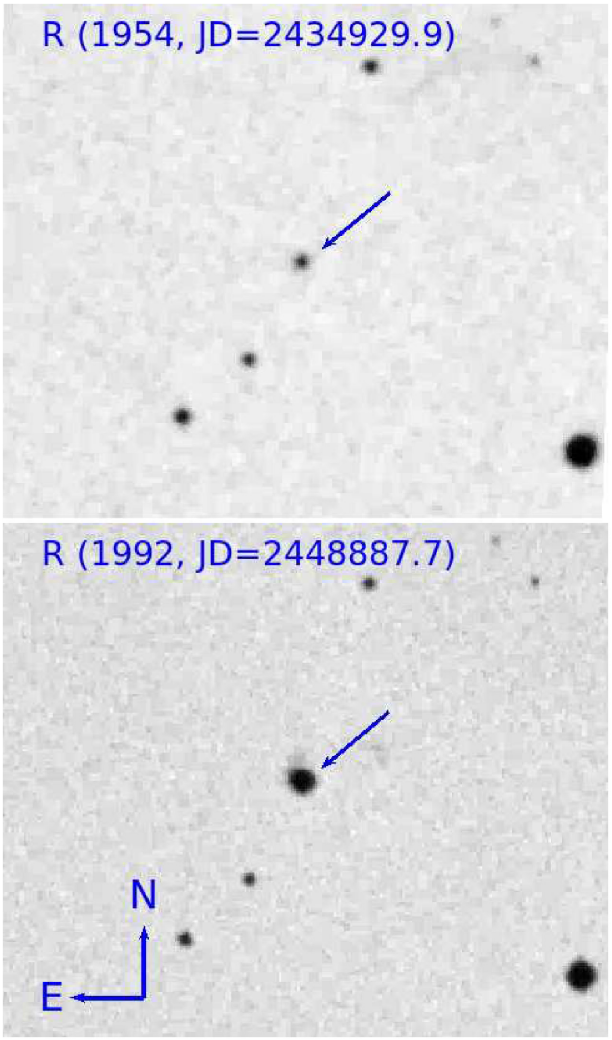

Figure 7. Comparison of the POSS-I E and POSS-II R 3 arcmin × 3 arcmin images of V3, obtained in 1954 and 1992, respectively. In both images, the variable star is marked by the blue arrow.

flat-spectrum sources). The concern arises from the fact that if the outbursts are ≃10 times more common during the Class I stage (see Section 6.1.1), then even a low contamination from Class I YSOs would result in a high fraction of our outbursts sources being from the embedded phase.

To study this effect we performed a deeper analysis of the likely evolutionary stage of the YSOs in our long-term outburst sample. From the nine YSOs in this sample, 8 were selected from the Marton et al. (2016) catalogue and given a Class II YSO classification using the Koenig & Leisawitz (2014) criteria, whilst V4 is selected from the near-IR excess as determined from its 2MASS colours. We determined the 2–24 μm spectral index, α, for the observed SED of the burst sample, using 2MASS and *WISE* magnitudes. Table 3 lists the values determined for the sample. We see that $\alpha \leq -0.3$ for four objects in the sample is consistent with the definition for Class II YSOs of Greene et al. (1994). For five objects, the spectral index indicates an earlier evolutionary stage.

For objects where α is consistent with a Class II stage, we find further evidence to support the idea that the envelope has dissipated and that these are pure disc-bearing objects. The interferometric ^{13}CO and C^{18}O survey of Fehér et al. (2017) determines that V10 (V733 Cep) and V2 (HBC722) have evolved beyond the Class I and flat-spectrum stages. Ábrahám et al. (2018) determine that the pre-outburst spectrum of V36 (V582 Aur) is that of a CTTS. There is no literature information in the case of V4, however the spectral index of $\alpha = -0.4$ is an upper limit and makes this object a very likely Class II YSO.

Table 3. Final sample of YSO outbursts.

ID	Name[a]	α	Envelope?
V1	V1057 Cyg	− 0.1	Yes (Fehér et al. 2017)
V2	HBC 722	− 0.44	No (Fehér et al. 2017)
V4	2M J0233 + 6156	− 0.4	?
V6	V350 Cep	− 0.17	Yes (Muzerolle et al. 2004)
V9	2M J0841 − 4052	− 0.23	?
V10	V733 Cep	− 0.78	No (Fehér et al. 2017)
V31	V960 Mon	− 0.19	Yes (Kóspál et al. 2015)
V36	V582 Aur	− 0.33	No (Ábrahám et al. 2018)
V51	WRAY 15-488	− 0.27	?

Note: [a] We do not present the SIMBAD ID of the variables stars from Table 2, but instead the column shows the most common name found in the literature.

In the case of objects with $\alpha > -0.3$, we find that V1 (V1057 Cyg) shows evidence for a large and dense envelope (Fehér et al. 2017), whilst the SED of V31 (V960 Mon) suggests the presence of an envelope in Kóspál et al. (2015). V6 (V350 Cep) is classified as a protostar candidate in Muzerolle et al. (2004, based also on the 70 μm magnitude of the YSO) and Miranda et al. (1994) establish that the object is embedded in nebulosity. Thus, these three YSOs were not included in our calculation of the outburst rate (see Section 6).

The value of spectral index for V9 and V51 is not within the Class II limits of the Greene et al. (1994) classification. However, the value is not far from those of Class II YSOs, and we note that we did not consider the effects of reddening in the calculation of α, which would likely place the objects in the Class II definition. In addition is hard to determine whether the slope of the SED has changed due to the outburst. In the case of V9, we find that from observations prior to outburst, the object is an Hα emission line star from Pettersson & Reipurth (1994). The authors provide a measure of the strength of the Hα line on a scale from 1 (faint) to 5 (very strong), where V9 was listed with I(Hα) = 3. We can estimate the equivalent width (EW), this corresponds to using objects from Pettersson & Reipurth (1994) with measured EWs which also have I(Hα) classes (see their table 3). YSOs that show the same value for the intensity of the emission line, have EWs that go between 10 and 100 Å with an average of 38 Å. Thus, is very likely that the progenitor of V9 is in fact a disc-bearing (Class II) YSO. Therefore the object was retained in the outburst sample for the remainder of our analysis. V51 was also originally classified as an emission line star prior to outburst (Wray 1966). In addition the object was classified as a CTTS (from it SED during outburst, see Appendix A3) by Gregorio-Hetem & Hetem (2002). Therefore, we included both objects in our sample of Class II outbursts. Thus, we have a final sample of six large-amplitude, long-time-scale accretion-driven Class II YSO outbursts.

6 OUTBURST RATE

To determine the time-scale of high-amplitude, long-lasting outbursts events during the Class II stage, we first obtained the baseline of observation for each YSO in our sample. Therefore, we queried the SSA data base for the epoch of observation for the corresponding

B, R1, R2, and I photographic plates. The baseline of observations for each star was given by the difference between the *Gaia* DR2 epoch (set at 2015.5) and that of the oldest photographic plate observation. The total time covered was calculated as the simple sum of all of the baselines, which yields 782 959 yr or a mean baseline of 55.6 yr.

We can place formal limits on the 'waiting time' (τ) between outbursts, provided that our model is that all YSOs have quiescent periods of order centuries or longer, punctuated by outbursts where the star rises by more than 4 mag on a time-scale of around a decade or less, and then remains bright for decades. If that is the case, then the probability of observing k rises, given an event rate for the whole sample of R yr^{-1}, and a total observation time t is given by the Poisson distribution

$$P(k|R) = \frac{(Rt)^k}{k!}\mathrm{e}^{-Rt}. \quad (3)$$

This is formally derived by considering the binomial distribution and approximating for low event rates. We are interested not in the event rate for the whole sample, but in the waiting time for a single star $\tau = 1/(RN)$. Substituting this into equation (3), we then used Bayes' theorem to derive the probability density function $p(\tau|k)$ of a particular waiting time τ, given k as

$$p(\tau|k) = \frac{p(\tau)P(k|\tau)}{P(k)} = \frac{p(\tau)}{P(k)}\frac{(Nt/\tau)^k}{k!}\mathrm{e}^{-Nt/\tau}. \quad (4)$$

We then evaluated $P(k)$ in the normal way as

$$P(k) = \int_{\tau=0}^{\infty}\frac{(Nt/\tau)^k\mathrm{e}^{-Nt/\tau}}{k!}p(\tau)\mathrm{d}\tau = \frac{Nt}{k(k-1)}p(\tau), \quad (5)$$

where we assumed that the prior is independent of τ (an assumption we shall return to later), and hence solved the integral using the Γ-function. This yielded the result that

$$p(\tau|k) = \frac{(Nt)^{k-1}}{(k-2)!\,\tau^k}\mathrm{e}^{-Nt/\tau}. \quad (6)$$

Differentiating this to find the turning point gave the unsurprising result that the most probable value of τ is given by

$$\tau = \frac{Nt}{k}. \quad (7)$$

We then calculated the confidence limits as the values of τ which enclosed the most likely 68 per cent of the probability given by equation (6). We achieved this by integrating equation (6) over all values of τ where p exceeded a certain value. We then decreased that value of p until the integral reached 0.68, at which point the extreme values of τ are our 68 precent confidence limits. Our observed values of $N = 14\,077$, $t = 55.6$ yr, and $k = 6$ gave $\tau = 131^{+91}_{-48}$ kyr (68 per cent confidence).

To test the effect of priors, we repeated the calculation using $p(r) \propto 1/\tau$, which gave

$$p(\tau|k) = \frac{(Nt)^k}{(k-1)!\,\tau^{k+1}}\mathrm{e}^{-Nt/\tau}, \quad (8)$$

and the most probable value of τ as

$$\tau = \frac{Nt}{(k+1)}. \quad (9)$$

These yielded $\tau = 112^{+68}_{-38}$ kyr (68 per cent confidence). The prior is equivalent to assuming that equal decades of τ have equal probabilities of containing τ. This is normally thought a more reasonable prior for a quantity which must be greater than zero, and so this is our preferred result, although the prior does not have a great impact.

6.1 Comparison with literature data

The number we obtain in the above analysis represents the first observational determination that long-lasting outbursts do in fact occur during the Class II stage and the frequency of such events. To our knowledge, there is only one other observational study, from Scholz et al. (2013), that provides an outburst recurrence time-scale for YSOs. However, our analysis differs from Scholz et al. (2013) as the authors do not divide their YSO sample into different classes.

In this subsection, we compare our results with that of Scholz et al. (2013) as well as comparing it with other observational and theoretical evidence that give some estimate of the frequency of YSO outbursts.

6.1.1 Scholz et al. (2013)

With the aim of determining the outburst recurrence time-scale in YSOs, Scholz et al. (2013) searched for young eruptive variables by comparing *Spitzer* with *WISE* photometry, thus providing a 5 yr baseline. The authors performed their analysis for about 8000 YSOs divided into two samples that were analysed separately. Sample A contains 4000 YSOs selected from c2d and clusters surveys (Gutermuth et al. 2009), with additional objects found in the NGC 2264, Taurus and North American/Pelican Nebulae regions. Sample B comprises YSOs found in the Robitaille et al. (2008) catalogue of intrinsically red objects, in which Scholz et al. (2013) find $\simeq$ 4000 YSOs.

In their analysis, Scholz et al. (2013) did not divide objects into different YSO classes, but we require such a division to compare their data with our results. According to the authors, sample A contains about 2800 Class II YSOs. In this sample, they detected one very likely outburst candidate, V2492 Cyg, which is a class I YSO (Kóspál et al. 2011). Given the lack of Class II outbursts, we cannot use the same arguments from Section 6 as the integral of equation (8) over $\tau > 0$ is not finite for $k = 0$. All we can say is that the outburst rate is probably longer than the monitored YSO years from sample A, i.e. $5 \times 2800 = 14$ kyr. From sample A, we can only estimate the outburst rate during the Class I stage. To obtain this, we have used the same $1/\tau$ prior we preferred in Section 6, but also note that without this prior we cannot obtain a confidence limit as the integral of equation (6) over $\tau > 0$ is not finite for $k = 1$. This yields a time-scale of $3.0^{+12.7}_{-1.9}$ kyr for the Class I stage.

In sample B, Scholz et al. (2013) find two outburst candidates, 2MASS J16443712−4604017 (hereafter SFW13 YSO1) and 2MASS J15111357−5902366 (hereafter SFW13 YSO2). Using the multi-epoch K_s photometry from the VISTA Variables in the Via Lactea survey and its extension (VVV and VVVX, respectively, see e.g. Saito et al. 2012; Bica et al. 2018) we determined that SFW13 YSO2 showed high-amplitude recurrent variability over the 2010–2018 period, whilst SFW13 YSO1 has remained at a bright state since 2010 until at least the latest epoch of VVVX (May 2018, see Fig. 8), making the YSO a true eruptive variable. Using the Koenig & Leisawitz (2014) classification criteria, we determined that SFW13 YSO1 is a Class II YSO from its *WISE* colours. However the object shows a rising SED (Fig. 8) with an spectral index, $\alpha = 0.12$ that is more consistent with a Class I YSO. Thus, we assume the latter classification for the object.

An analysis of near- to mid-IR colours of candidate YSOs from red objects in Robitaille et al. (2008) show that $\simeq$ 40 per cent can

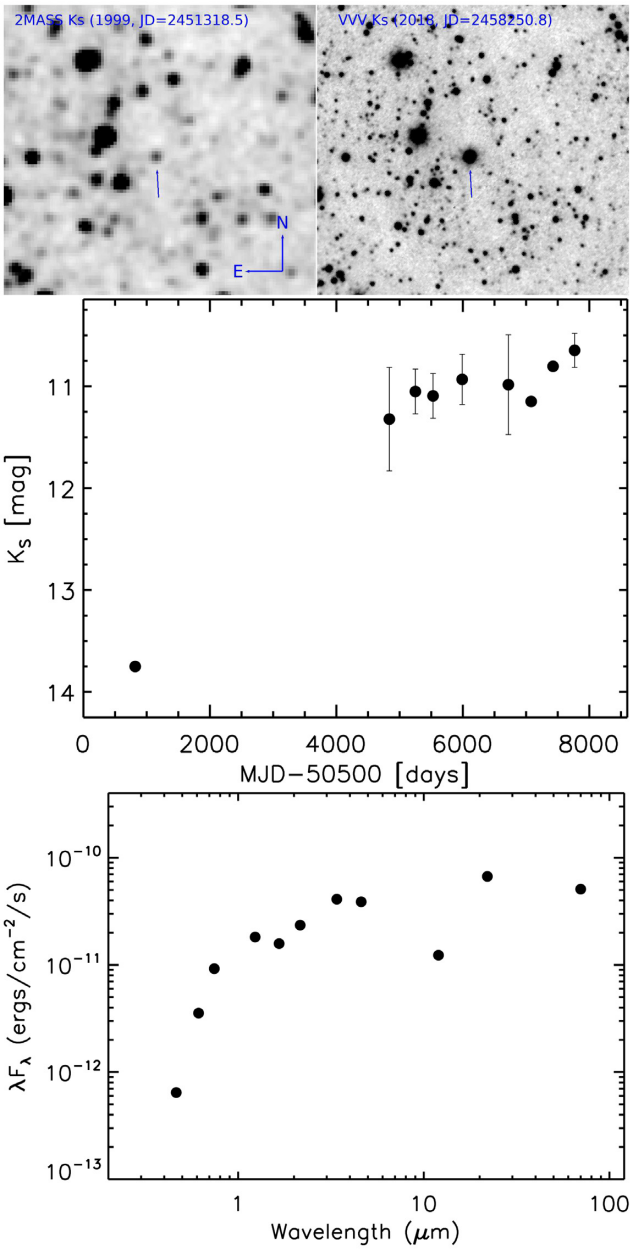

Figure 8. Top: comparison of 1.5 arcmin × 1.6 arcmin K_S images for SFW13 YSO1 from 2MASS (left) and VVVX (right). In both images, the YSO is marked by a blue arrow. Middle: K_S light curve of SFW13 YSO1 arising from 2MASS, VVV, and VVVX. The object is close to the saturation limit in the VVV and VVVX images and thus suffers from non-linearity effects, making the individual data points unreliable. Given this, for VVV and VVVX, we averaged the photometry for each observing campaign. The error bars mark the standard deviation from the average. Bottom: SED of SFW13 YSO1.

be classified as class II YSOs. Assuming the same fraction for sample B in Scholz et al. (2013) implies that around 1600 objects are Class II YSOs. Since the only outburst in sample B, SFW13 YSO1, is more likely a Class I YSO, we can only estimate that the recurrence time-scale in the Class I stage, using the $1/\tau$ prior, of $6.0^{+25.3}_{-3.9}$kyr. Similarly to the results of sample A, we can only say that the outburst recurrence time-scale during the Class II stage is longer than $\simeq$8 kyr.

The lack of Class II outbursts in the samples of Scholz et al. (2013) agrees with the results from our work, i.e. given the outburst rate determined by us we would not expect to observe an outburst for a sample of a few thousand class II YSOs over a 5 yr baseline.

The analysis of the Scholz et al. (2013) yields another important result, as samples A and B show that during the Class I stage, outbursts due to variable accretion appear to be $\approx$10 times more frequent than during the Class II phase.

6.1.2 *Theoretical estimate*

Bae et al. (2014) find that GI-induced spiral density waves can heat the inner disc and trigger magnetorotational instabilities (MRI) that will lead to accretion outbursts (or GI + MRI mechanism). They find that this process is more efficient at earlier stages when the envelope dominates the disc, with the number of outbursts decreasing as the star approaches the post-infall phase. Based on fig. 3 of Bae et al. (2014), Hillenbrand & Findeisen (2015) estimate an outburst rate of 8×10^{-5} yr^{-1} star^{-1} during the class I stage, and 3×10^{-6} yr^{-1} star^{-1} during the Class II stage, or a recurrence time-scale of 12.5 and 333 kyr, respectively. The value for the Class I stage is consistent with our class I estimates. The theoretical estimate for the Class II stage agrees with our results in the fact that is much longer than that of the Class I stage, and that outburst occur over scales longer than 100 kyr. However, it is still longer than the recurrence time-scale from our study, and is formally rejected at a 95.3 per cent confidence level.

6.1.3 *Other observational evidence*

The recurrence time-scale from our study is larger than the time between ejection events of $\simeq$1000 yr determined from the observed gaps between H_2 knots along jets from YSOs (Ioannidis & Froebrich 2012; Froebrich & Makin 2016; Makin & Froebrich 2018) and the 100 yr time-scale observed in MNors by Contreras Peña et al. (2017a). However this is not surprising as H_2 jets likely trace the accretion related events during the Class I phase (Ioannidis & Froebrich 2012) and that the young eruptive variables in Contreras Peña et al. (2017a) are biased towards Class I YSOs.

Fischer, Safron & Megeath (2019) studied the large-amplitude mid-IR variability for a sample of 319 protostars (YSOs with class designations 0, I, or flat) in Orion, by comparing *Spitzer* versus *WISE* photometry. Based on the recovery of two outbursts over the 6.5 yr baseline, Fischer et al. (2019) determine an outburst rate of 1000 yr with a 90 per cent confidence interval of 690–40 300 yr. This agrees with our results that suggest that outbursts are more frequent towards YSOs at earlier evolutionary stages the Class II stage.

6.1.4 *Gaia17bpi and the rate from the* Gaia *alerts*

At the time of writing, Hillenbrand et al. (2018), based on photometry from *Gaia*, reported the discovery of a new YSO outburst that has the characteristics of the most powerful events. The outburst occurred around 2014 and is still ongoing, so it may well be a long-lasting event. The YSO prior to outburst was faint at $r = 22$ mag and it is difficult to classify the source from its SED, but it could correspond to a Class II YSO (see fig. 2 of Hillenbrand et al. 2018).

The discovery of a potential Class II YSO outburst over the 3 yr baseline of *Gaia* does not contradict our results. Given an outburst rate of 112 kyr, to observe an outburst over a 3 yr baseline

would imply that we are observing a sample of approximately 40000 YSOs. This is conceivable if we take into account that there is a large population of YSOs that are too faint for current and past surveys. The number of YSOs increases as we go towards fainter magnitudes (see e.g. Contreras Peña et al. 2017a) and Gaia17bpi itself was in fact unknown prior to its outburst. Hillenbrand et al. (2018) followed up the YSO as a *Gaia* alert (Hodgkin et al. 2013) was triggered on a source that was found in proximity of a star-forming region.

The outburst of Gaia17bpi is remarkable as the analysis of Hillenbrand et al. (2018) shows that the outburst started first at mid-IR wavelengths, with the optical outburst occurring at least a year later. This is consistent with instabilities the lead to an 'outside–in' type outburst, which is predicted by the outburst mechanisms that could explain outbursts during the Class II stage (see Section 8).

7 CAVEATS

7.1 Contamination by other classes of variable stars

The process of planet formation is more likely to be affected by long-lasting rather than short-term accretion events. In this sense, we needed to be careful not to include objects that go through sudden episodes of large changes in the accretion rate, but with a short duration. For example, V8 is the known short-term eruptive YSO ASASSN13-db (Sicilia-Aguilar et al. 2017). When inspecting its long-baseline light curve the object did not resemble a long-lasting outburst, but instead appeared to be irregular, i.e. going from bright to faint states repetitively across time. As a result we are confident that similar objects that suffer short-term accretion events were not included in our final sample of long-lasting YSO outbursts.

The classification of high-amplitude variable stars as showing long-lasting outbursts, based only on the photometric properties of the sample, also has the risk of selecting objects with light curves that can mimic an accretion-related outburst, especially if the light curve sampling is sparse (as discussed in Section 5.2). For example is not hard to imagine that sparse sampling of objects brightening from high-amplitude, long-lasting eclipses by inhomogeneities at long distances in the accretion disc (RW Aur, and AA Tau) or a precessing disc in a binary system (e.g. KH 15D, Aronow et al. 2018) could resemble a YSO outburst.

Contemporaneous multicolour monitoring and/or spectroscopic follow-up are usually used to determine that the dramatic change in the brightness of the system is due to large changes in the accretion rate. The sample of six long-lasting YSO outbursts that were used to determine the outburst rate in Section 6 contains three known YSO outbursts that have been confirmed as such via spectroscopic follow up (V2, V10, and V36). Hence, in this work, we have identified three previously unknown outbursting YSOs that are included in our calculation. Of these, V51 has literature data confirming that this object is an eruptive YSO (see Appendix A3). Recent spectroscopic monitoring shows that V4 has the spectroscopic characteristics of objects at the high accretion rates of long-lasting YSO outbursts (Contreras Peña et al., in preparation). V9 is the only object lacking such an spectroscopic confirmation.

However, as discussed in Section 5.2, we tried to avoid including objects where identification as long-lasting YSO outburst was uncertain due to bad sampling and/or lack of additional data from the literature. As a result, we are likely excluding objects that could mimic strong YSO outbursts.

7.2 Non-YSO contamination

The sources of contamination in the classification of YSOs arises from red extragalactic sources, such as obscured AGNs, and Galactic sources, mainly reddened giant stars or dust-enshrouded asymptotic giant branch stars (see e.g Robitaille et al. 2008; Povich et al. 2013). However, we do not expect the contamination in our sample to be high, as most of our objects arise from samples where contaminants had already been dealt with. For example, Marton et al. (2016) estimate a less than 1 per cent contamination in their sample of YSOs, whilst this number is not larger than 2 per cent in the samples of Megeath et al. (2012) and Gutermuth et al. (2009).

We could expect a higher percentage of contamination from the sample of objects that are classified using ALLWISE photometry. Koenig & Leisawitz (2014) establish that a contamination of 7 per cent is expected in objects classified as Class II YSOs from ALLWISE photometry. If we assume that objects classified from ALLWISE or 2MASS photometry alone (6419 objects) suffer this high contamination, and that objects selected from other methods suffer a 1 per cent contamination, then we expect $\simeq$492 or 3.5 per cent of objects are contaminants in our sample.

7.3 Misclassification

The likely evolutionary stage for the majority of our sample was determined using the Koenig & Leisawitz (2014) criteria. Inspection of their fig. 5 shows that the area in the colour–colour plane that defines the Class II YSOs could be contaminated by objects at earlier evolutionary stages, i.e. flat-spectrum and Class I sources. Given the much higher outburst rate of Class I sources compared with Class II (Section 6.1.1), even a small percentage of misclassification would lead to the detection of Class I YSOs in our outburst sample, an effect that we observed in our results (see Section 5.4).

To estimate this contamination, we obtained ALLWISE photometry for a sample of YSOs from Megeath et al. (2012) that also have measured values of the spectral index, α. Then we applied the Koenig & Leisawitz (2014) criteria to determine the likely evolutionary stage of these YSOs. Finally, we compared the latter with the stage determined from α. We found that 7 per cent of objects classified as Class II YSOs from the Koenig & Leisawitz (2014) criteria are classified as being at earlier evolutionary stages from the value of the spectral index. As we will show in the following, this estimate is consistent with the number of Class I YSO outburst that contaminate our sample in Section 5.4

7.4 Effects of contamination and misclassification on the outburst rate

We can now examine the effect of all of the uncertainties discussed in Sections 7.1–7.3 on our outburst rate. If we first only consider the effect of the lack of spectroscopic confirmation as an accretion outburst for V9 (Section 7.1), then our outburst sample reduces from 6 to 5 objects. This implies an increase of the outburst rate, from 112 to 130 kyr.

Considering possible contamination of non-YSOs, our sample reduces to 13 589 objects (see Section 7.2). If we further consider a 7 per cent contamination from Class I YSOs (951 objects, see Section 7.3) then we are left with 12 638 Class II YSOs. If we use a sample of six YSO outbursts, the outburst rate in Class II

YSOs reduces from 112 to 100 kyr. If we omittV9, the outburst rate increases again to 117 kyr.

Thus considering all of the possible contamination and exclusion effects, the outburst rate changes to between 100 and 130 kyr. This is a change that is within the 68 per cent confidence intervals we estimated in Section 6.

We can also use the contamination of Class I YSOs to determine another approximate estimate of the outburst rate in the Class I stage. In Section 5.4, we found that 3 YSO outbursts are more likely to be Class I YSOs, if we consider a total sample of 1043 Class I YSOs implies an outburst rate of 13^{+15}_{-6} kyr (68 per cent confidence, assuming the $1/\tau$ prior). This number agrees remarkably well with that estimated from the Scholz et al. (2013) YSO sample.

7.5 Selection criteria

The value for the recurrence time-scale derived from our sample of Class II YSO outbursts is subject to some caveats from the initial selection. As we are interested in a statistical characterization of variability, we should not use variability as a selection criterion. However, is clear that some of the objects in our initial catalogue were initially identified because of their variability, primarily the FU∗ and or∗ classes. However given the need of IR data to identify Class II objects, we believe that they would have also have been identified as YSOs in these surveys, regardless of their variability. Hence, we left them in the sample.

8 OUTBURST MECHANISM

The results from our analysis show for the first time that the suggestion that the frequency of the outbursts is lower in the Class II stage than during the Class I stage is correct. This has implications for the physical mechanism likely to be driving the outbursts during Class II phase.

As noted above GI + MRI instabilities become less efficient in disc dominated systems (Bae et al. 2014). Due to GI, and provided that the cooling time is shorter than the dynamical time-scale, disc pressure is not able to support the collapsing gas against its own gravity, leading to disc fragmentation (see e.g. Vorobyov & Basu 2005; Machida, Inutsuka & Matsumoto 2011). The fragments are later transported to the inner disc via gravitational interactions with the spiral arms (Machida et al. 2011), and are likely to trigger mass accretion bursts (Vorobyov & Basu 2010). This process is more efficient during the embedded phase. Mass accretion outbursts could occur during the Class II phase, but it is not clear whether these fragments survive beyond the embedded stage (see Audard et al. 2014). Zhu, Hartmann & Gammie (2010) find that for the lower infall rates of Class II objects, layered MRI turbulence might be able to accumulate mass and trigger the MRI outbursts. However, these bursts are likely of lower amplitude and of shorter duration (Audard et al. 2014).

Lodato & Clarke (2004) propose that the interaction of a massive planet with the disc can trigger thermal instabilities in the outer disc. In this scenario, the migration of the planet opens up a gap in the disc, and the inner disc is emptied out. Due to the tidal effect induced by the planet, material will pile up at larger radii. When the density reaches a critical value, the thermal instability is triggered. A final possibility is that the gravitational force of a companion star may perturb the disc and thus enhance accretion (Bonnell & Bastien 1992). This idea is supported by the fact that a number of known eruptive variables are members of binary systems (see e.g. Fedele et al. 2007; Reipurth, Herbig & Aspin 2010; Caratti o Garatti et al. 2015). In some of these, both stars in the system are found to have characteristics of strong accretors (e.g. systems AR6A + B, RNO1B/C; Aspin & Reipurth 2003).

Therefore, the planet-induced thermal instability and binary models are most likely to explain the existence of large accretion events during the Class II stage. However, we note that the fact that more than one mechanism can explain the outbursts has implications for our interpretation of the outburst rate. As noted by Scholz et al. (2013), if outbursts are triggered by two or more different mechanisms not all of which might apply to every YSO (such as outbursts due to encounters in multiple systems) would imply that the frequency of outbursts is highly variable amongst young stars, and it would not be valid to extrapolate the outburst rate for a single YSO from our estimated Class II recurrence time-scale.

9 SUMMARY

In this work, we compared the all-sky digitized photographic plate surveys provided by SuperCOSMOS with the latest data release from *Gaia* (DR2) for a large sample of YSOs. The mean baseline of 55 yr implies that we monitored ≃800 000 YSO years.

We retrieved 139 high-amplitude variables with $\Delta R \geq 1$ mag. We believe we are complete for amplitudes larger than 2 mag. In Section 5, we determined that most of the variable stars are found with amplitudes between 1 and 3 mag, where variable extinction or extreme changes due to hotspot variability are the likely mechanisms driving the variability in these YSOs. For amplitudes larger than 3 mag, we also find objects with apparent long-lasting fading events, likely related to extinction, and objects with irregular variability. At these larger amplitudes, the latter are more likely explained by short-term accretion events that appear as irregular given the long baseline of the light curves.

YSOs with this extreme variability, but not related to variable accretion, are interesting in their own right. For example, long-lasting fading events could be explained by extinction due to inhomogeneities at large distances in the disc, which can relate to planet-formation processes.

Objects where variability could be due to changes in the accretion rate, but with outburst duration that is less than 10 yr, were not included in the calculation of the recurrence time-scale of outbursts in the Class II stage. This is because short-duration outbursts are less likely to have an impact on the formation and evolution of protoplanets Hubbard (see e.g. 2017b).

We classified nine YSOs as showing long-term accretion driven outbursts, with three of them representing new discoveries (Section 5.3). We discussed the possible contamination by Class I YSOs and we determine that three objects in this group are more likely at a younger evolutionary stage. Therefore, six YSOs are left in our final sample of Class II YSO outbursts (Section 5.4).

In Section 6, we determined, for the first time, that long-term accretion-driven outbursts occur during the Class II stage of young stellar evolution. The frequency of these events was found at $\tau = 112^{+68}_{-38}$ kyr (68 per cent confidence). Our results imply that planet formation models must take into account the likely effects that these episodic accretion events can have on the formation and evolution of planetary systems.

Through the analysis of the YSO sample of Scholz et al. (2013, see Section 6.1.1) as well as possible contamination of Class I YSOs in our sample (Section 7.4), we have estimated the recurrence

time-scale of accretion driven outbursts at this earlier evolutionary stage. We found that episodic accretion events are ≃10 times more frequent than during the Class II stage, in agreement with theoretical expectations.

ACKNOWLEDGEMENTS

This work has made use of data from the European Space Agency (ESA) mission *Gaia* (https://www.cosmos.esa.int/gaia), processed by the *Gaia* Data Processing and Analysis Consortium (DPAC, https://www.cosmos.esa.int/web/gaia/dpac/consortium). This research has made use of the NASA/ IPAC Infrared Science Archive, which is operated by the Jet Propulsion Laboratory, California Institute of Technology, under contract with the National Aeronautics and Space Administration. Funding for the DPAC has been provided by national institutions, in particular the institutions participating in the *Gaia* Multilateral Agreement. The contributions of CCP and TN were funded by a Leverhulme Trust Research Project Grant and of SM through a Science and Technology Facilities Council (STFC) studentship. We are grateful to N. Hambly for his help in understanding the SSS data base.

REFERENCES

Ábrahám P. et al., 2018, ApJ, 853, 28
Alam S. et al., 2015, ApJS, 219, 12
Alfonso-Garzón J., Domingo A., Mas-Hesse J. M., Giménez A., 2012, A&A, 548, A79
Allen T. S. et al., 2012, ApJ, 750, 125
Aronow R. A., Herbst W., Hughes A. M., Wilner D. J., Winn J. N., 2018, AJ, 155, 47
Aspin C., Reipurth B., 2003, AJ, 126, 2936
Audard M. et al., 2014, in Beuther H., Klessen R. S., Dullemond C. P., Henning Th., eds, Protostars and Planets VI. Univ. Arizona Press, Tucson, AZ, p. 387
Bae J., Hartmann L., Zhu Z., Nelson R. P., 2014, ApJ, 795, 61
Barentsen G., et al., 2014, MNRAS, 444, 3230
Barsony M., Haisch K. E., Marsh K. A., McCarthy C., 2012, ApJ, 751, 22
Baruteau C., Papaloizou J. C. B., 2013, ApJ, 778, 7
Béjar V. J. S., Zapatero Osorio M. R., Rebolo R., 2004, Astron. Nachr., 325, 705
Bell C. P. M., Naylor T., Mayne N. J., Jeffries R. D., Littlefair S. P., 2013, MNRAS, 434, 806
Bica E., Minniti D., Bonatto C., Hempel M., 2018, PASA, 35, e025
Billot N., Noriega-Crespo A., Carey S., Guieu S., Shenoy S., Paladini R., Latter W., 2010, ApJ, 712, 797
Boley A. C., Morris M. A., Ford E. B., 2014, ApJ, 792, L27
Bonnell I., Bastien P., 1992, ApJ, 401, L31
Bouvier J., Grankin K., Ellerbroek L. E., Bouy H., Barrado D., 2013, A&A, 557, A77
Bouy H., Alves J., Bertin E., Sarro L. M., Barrado D., 2014, A&A, 564, A29
Bozhinova I. et al., 2016, MNRAS, 463, 4459
Cannon R. D., 1984, in Capaccioli M., ed., Astrophysics and Space Science Library Vol. 110, IAU Colloq. 78: Astronomy with Schmidt-Type Telescopes. D. Reidel Publishing Co., Dordrecht, p. 25
Caratti o Garatti A. et al., 2015, ApJ, 806, L4
Carmona A., van den Ancker M. E., Audard M., Henning T., Setiawan J., Rodmann J., 2010, A&A, 517, A67
Carpenter J. M., Hillenbrand L. A., Skrutskie M. F., 2001, AJ, 121, 3160
Carpenter J. M., Hillenbrand L. A., Skrutskie M. F., Meyer M. R., 2002, AJ, 124, 1001
Chambers J., 2014, Science, 344, 479
Chambers K. C. et al., 2016, preprint (arXiv:1612.05560)
Chavarría L. A., Allen L. E., Hora J. L., Brunt C. M., Fazio G. G., 2008, ApJ, 682, 445
Cieza L. A. et al., 2016, Nature, 535, 258
Cody A. M., Hillenbrand L. A., 2010, ApJS, 191, 389
Cody A. M., Hillenbrand L. A., David T. J., Carpenter J. M., Everett M. E., Howell S. B., 2017, ApJ, 836, 41
Connelley M., Reipurth B., 2018, ApJ, 861, 145
Connelley M. S., Reipurth B., Tokunaga A. T., 2008, AJ, 135, 2496
Contreras Peña C. et al., 2017a, MNRAS, 465, 3011
Contreras Peña C. et al., 2017b, MNRAS, 465, 3039
Cutri R. M. et al., 2013, VizieR Online Data Catalog, p. 2328, http://adsabs.harvard.edu/abs/2013yCat.2328....0C
Da Rio N., Robberto M., Soderblom D. R., Panagia N., Hillenbrand L. A., Palla F., Stassun K., 2009, ApJS, 183, 261
Dahm S. E., Hillenbrand L. A., 2015, AJ, 149, 200
Dahm S. E., Simon T., 2005, AJ, 129, 829
Davies C. L., Kreplin A., Kluska J., Hone E., Kraus S., 2018, MNRAS, 474, 5406
Djorgovski S. G. et al., 2011, preprint (arXiv:1102.5004)
Dolan C. J., Mathieu R. D., 2002, AJ, 123, 387
Drew J. E. et al., 2014, MNRAS, 440, 2036
Droege T. F., Richmond M. W., Sallman M. P., Creager R. P., 2006, PASP, 118, 1666
Dunham M. M. et al., 2014, Beuther H., Klessen R. S., Dullemond C. P., Henning Th., Protostars and Planets VI. Univ. Arizona Press, Tucson, AZ, p. 195
Epchtein N. et al., 1994, Ap&SS, 217, 3
Evans N. J., II et al., 2003, PASP, 115, 965
Evans N. J., II et al., 2009, ApJS, 181, 321
Fazio G. G. et al., 2004, ApJS, 154, 10
Fedele D., van den Ancker M. E., Petr-Gotzens M. G., Rafanelli P., 2007, A&A, 472, 207
Fehér O., Kóspál Á., Ábrahám P., Hogerheijde M. R., Brinch C., 2017, A&A, 607, A39
Feigelson E. D. et al., 2013, ApJS, 209, 26
Fischer W. J., Safron E., Megeath S. T., 2019, ApJ, 872, 183
Frasca A., Biazzo K., Alcalá J. M., Manara C. F., Stelzer B., Covino E., Antoniucci S., 2017, A&A, 602, A33
Froebrich D. et al., 2018, MNRAS, 478, 5091
Froebrich D., Makin S. V., 2016, MNRAS, 462, 1444
Gaia Collaboration et al., 2018, A&A, 616, A1
Garaud P., Lin D. N. C., 2007, ApJ, 654, 606
Grankin K. N., Melnikov S. Y., Bouvier J., Herbst W., Shevchenko V. S., 2007, A&A, 461, 183
Greene T. P., Wilking B. A., Andre P., Young E. T., Lada C. J., 1994, ApJ, 434, 614
Gregorio-Hetem J., Hetem A., 2002, MNRAS, 336, 197
Gregorio-Hetem J., Lepine J. R. D., Quast G. R., Torres C. A. O., de La Reza R., 1992, AJ, 103, 549
Gutermuth R. A. et al., 2008, ApJ, 674, 336
Gutermuth R. A., Megeath S. T., Myers P. C., Allen L. E., Pipher J. L., Fazio G. G., 2009, ApJS, 184, 18
Hackstein M. et al., 2015, Astron. Nachr., 336, 590
Hambly N. C. et al., 2001, MNRAS, 326, 1279
Hartmann L., Kenyon S. J., 1987, ApJ, 322, 393
Hartmann L., Kenyon S. J., 1996, ARA&A, 34, 207
Henden A. A., Levine S., Terrell D., Welch D. L., 2015, in American Astronomical Society Meeting Abstracts #225. p. 336.16
Herbig G. H., Bell K. R., 1988, Third Catalog of Emission-Line Stars of the Orion Population: 3, Lick Observatory, Santa Cruz
Herbig G. H., Dahm S. E., 2002, AJ, 123, 304
Herbst W., Shevchenko V. S., 1999, AJ, 118, 1043
Herbst W., Herbst D. K., Grossman E. J., Weinstein D., 1994, AJ, 108, 1906
Hernández J. et al., 2007, ApJ, 662, 1067
Hernández J. et al., 2014, ApJ, 794, 36
Hillenbrand L., 2014, Astron. Telegram, 6797, 1
Hillenbrand L. A., Findeisen K. P., 2015, ApJ, 808, 68

Hillenbrand L. A. et al., 2013, AJ, 145, 59
Hillenbrand L. A. et al., 2018, ApJ, 869, 146
Hodgkin S. T., Wyrzykowski L., Blagorodnova N., Koposov S., 2013, Philos. Trans. R. Soc. Lond. Ser. A, 371, 20120239
Hsu W.-H., Hartmann L., Allen L., Hernández J., Megeath S. T., Mosby G., Tobin J. J., Espaillat C., 2012, ApJ, 752, 59
Hubbard A., 2017a, MNRAS, 465, 1910
Hubbard A., 2017b, ApJ, 840, L5
Hubbard A., Ebel D. S., 2014, Icarus, 237, 84
Ibryamov S., Semkov E., Peneva S., 2014, Res. Astron. Astrophys., 14, 1264
Ida S., Lin D. N. C., 2004, ApJ, 616, 567
Ioannidis G., Froebrich D., 2012, MNRAS, 425, 1380
Joy A. H., 1945, ApJ, 102, 168
Kafka S., Weaver J., Silvis G., Beck S., 2018, in American Astronomical Society Meeting Abstracts #231. p. 362.15
Kennedy G. M., Kenyon S. J., 2008, ApJ, 673, 502
Kenyon M. J., Jeffries R. D., Naylor T., Oliveira J. M., Maxted P. F. L., 2005, MNRAS, 356, 89
King R. R., Naylor T., Broos P. S., Getman K. V., Feigelson E. D., 2013, ApJS, 209, 28
Kirk J. M. et al., 2009, ApJS, 185, 198
Koenig X. P., Allen L. E., 2011, ApJ, 726, 18
Koenig X. P., Leisawitz D. T., 2014, ApJ, 791, 131
Koenig X. P., Allen L. E., Gutermuth R. A., Hora J. L., Brunt C. M., Muzerolle J., 2008, ApJ, 688, 1142
Kóspál Á. et al., 2011, A&A, 527, A133
Kóspál Á., Ábrahám P., Moór A., Haas M., Chini R., Hackstein M., 2015, ApJ, 801, L5
Kwon J., Tamura M., Hough J. H., Nakajima Y., Nishiyama S., Kusakabe N., Nagata T., Kandori R., 2015, ApJS, 220, 17
Lada C. J., 1987, in Peimbert M., Jugaku J., eds, IAU Symp. Vol. 115, Star Forming Regions. Kluwer, Dordrecht,p. 1
Lamm M. H., Bailer-Jones C. A. L., Mundt R., Herbst W., Scholz A., 2004, A&A, 417, 557
Lawrence A. et al., 2007, MNRAS, 379, 1599
Law N. M. et al., 2009, PASP, 121, 1395
Lee H.-T., Chen W. P., 2007, ApJ, 657, 884
Lodato G., Clarke C. J., 2004, MNRAS, 353, 841
Lubow S. H., Martin R. G., 2016, ApJ, 817, 30
Lucas P. W. et al., 2008, MNRAS, 391, 136
Machida M. N., Inutsuka S.-i., Matsumoto T., 2011, ApJ, 729, 42
Magakian T. Y., Movsesian T. A., Hovhannesian E. R., 1999, Astrophysics, 42, 121
Makin S. V., Froebrich D., 2018, ApJS, 234, 8
Marton G., Tóth L. V., Paladini R., Kun M., Zahorecz S., McGehee P., Kiss C., 2016, MNRAS, 458, 3479
Mayne N. J., Naylor T., Littlefair S. P., Saunders E. S., Jeffries R. D., 2007, MNRAS, 375, 1220
Megeath S. T. et al., 2012, AJ, 144, 192
Meingast S. et al., 2016, A&A, 587, A153
Meyer M. R., Calvet N., Hillenbrand L. A., 1997, AJ, 114, 288
Miller A. A. et al., 2011, ApJ, 730, 80
Minkowski R. L., Abell G. O., 1963, The National Geographic Society-Palomar Observatory Sky Survey. The University of Chicago Press, Chicago, IL, p. 481
Minniti D., Lucas P., VVV Team, 2017, VizieR Online Data Catalog. p. II/348 https://ui.adsabs.harvard.edu/#abs/2017yCat.2348....0M
Miranda L. F., Eiroa C., Fernandez M., Gomez de Castro A. I., 1994, A&A, 281, 864
Morales-Calderón M. et al., 2011, ApJ, 733, 50
Mordasini C., Mollière P., Dittkrist K.-M., Jin S., Alibert Y., 2015, Int. J. Astrobiol., 14, 201
Morgan D. H., Tritton S. B., Savage A., Hartley M., Cannon R. D., 1992, in MacGillivray H. T., Thomson E. B., eds, Astrophysics and Space Science Library Vol. 174, Digitised Optical Sky Surveys, Kluwer Academic Publishers, Dordrecht, p. 11
Muiños J. L., Evans D. W., 2014, Astron. Nachr., 335, 367
Mulders G. D., Pascucci I., Apai D., 2015, ApJ, 798, 112
Muzerolle J. et al., 2004, ApJS, 154, 379
Ochsenbein F., Bauer P., Marcout J., 2000, A&AS, 143, 23
Ofek E. O. et al., 2012, PASP, 124, 854
Panwar N., Chen W. P., Pandey A. K., Samal M. R., Ogura K., Ojha D. K., Jose J., Bhatt B. C., 2014, MNRAS, 443, 1614
Peña Ramírez K., Béjar V. J. S., Zapatero Osorio M. R., Petr-Gotzens M. G., Martín E. L., 2012, ApJ, 754, 30
Pettersson B., Reipurth B., 1994, A&AS, 104, 233
Pfalzner S. et al., 2015, Phys. Scr, 90, 068001
Pojmanski G., 2002, Acta Astron., 52, 397
Povich M. S. et al., 2013, ApJS, 209, 31
Rebull L. M., Hillenbrand L. A., Strom S. E., Duncan D. K., Patten B. M., Pavlovsky C. M., Makidon R., Adams M. T., 2000, AJ, 119, 3026
Rebull L. M. et al., 2010, ApJS, 186, 259
Rebull L. M. et al., 2011, ApJS, 193, 25
Reid I. N. et al., 1991, PASP, 103, 661
Reipurth B., Herbig G., Aspin C., 2010, AJ, 139, 1668
Reipurth B., Aspin C., Beck T., Brogan C., Connelley M. S., Herbig G. H., 2007, AJ, 133, 1000
Rice T. S., Reipurth B., Wolk S. J., Vaz L. P., Cross N. J. G., 2015, AJ, 150, 132
Rieke G. H. et al., 2004, ApJS, 154, 25
Rigliaco E., Natta A., Randich S., Testi L., Biazzo K., 2011, A&A, 525, A47
Rivera-Ingraham A., Martin P. G., Polychroni D., Moore T. J. T., 2011, ApJ, 743, 39
Robitaille T. P., Whitney B. A., Indebetouw R., Wood K., Denzmore P., 2006, ApJS, 167, 256
Robitaille T. P. et al., 2008, AJ, 136, 2413
Saito R. K. et al., 2012, A&A, 537, A107
Sandell G., Weintraub D. A., 2001, ApJS, 134, 115
Scholz A., Froebrich D., Wood K., 2013, MNRAS, 430, 2910
Semkov E. H., Peneva S. P., Munari U., Milani A., Valisa P., 2010, A&A, 523, L3
Sherry W. H., Walter F. M., Wolk S. J., 2004, AJ, 128, 2316
Sicilia-Aguilar A. et al., 2017, A&A, 607, A127
Skrutskie M. F. et al., 2006, AJ, 131, 1163
Spezzi L., Petr-Gotzens M. G., Alcalá J. M., Jørgensen J. K., Stanke T., Lombardi M., Alves J. F., 2015, A&A, 581, A140
Stecklum B., Linz H., 2013, in Protostars and Planets VI Posters
Suárez O., García-Lario P., Manchado A., Manteiga M., Ulla A., Pottasch S. R., 2006, A&A, 458, 173
Sung H., Bessell M. S., Chun M.-Y., 2004, AJ, 128, 1684
Tsujimoto M., Koyama K., Kobayashi N., Goto M., Tsuboi Y., Tokunaga A. T., 2003, AJ, 125, 1537
Venuti L. et al., 2014, A&A, 570, A82
Vereshchagin S. V., Chupina N. V., 2011, Astron. Rep., 55, 123
Vorobyov E. I., Basu S., 2005, ApJ, 633, L137
Vorobyov E. I., Basu S., 2006, ApJ, 650, 956
Vorobyov E. I., Basu S., 2010, ApJ, 719, 1896
Vorobyov E. I., Basu S., 2015, ApJ, 805, 115
Wackerling L. R., 1970, MmRAS, 73, 153
Wenger M. et al., 2000, A&AS, 143, 9
West R. M., 1984, in Capaccioli M., ed., Astrophysics and Space Science Library Vol. 110, IAU Colloq. 78: Astronomy with Schmidt-Type Telescopes, Kluwer, Dordrecht. p. 13
Wiramihardja S. D., Kogure T., Yoshida S., Ogura K., Nakano M., 1989, PASJ, 41, 155
Wolf C. et al., 2018, PASA, 35, e010
Woźniak P. R. et al., 2004, AJ, 127, 2436
Wray J. D., 1966, PhD thesis, Northwestern University
Wright E. L. et al., 2010, AJ, 140, 1868
Wurm G., Haack H., 2009, Meteorit. Planet. Sci., 44, 689
Wyrzykowski L., Hodgkin S., Blogorodnova N., Koposov S., Burgon R., 2012, 2nd Gaia Follow-up Network for Solar System Objects, p. 21, preprint (arXiv:1210.5007)
Zhu Z., Hartmann L., Gammie C., 2010, ApJ, 713, 1143

SUPPORTING INFORMATION

Supplementary data are available at *MNRAS* online.

Table 1. Example of the photometry obtained for each high-amplitude variable. In the tables we present the modified Julian date of the observations (estimated from the Julian date as MJD = JD−2400000.5), the *R*- or *r*-band magnitudes and the survey from where they are obtained. In the last column, we present a note depending on whether the magnitudes are an upper limit or if these result from transforming between different filters (marked as approximate in the table).
Table 2. The 139 high-amplitude variable stars detected in our analysis.

Please note: Oxford University Press is not responsible for the content or functionality of any supporting materials supplied by the authors. Any queries (other than missing material) should be directed to the corresponding author for the article.

APPENDIX A: INDIVIDUAL NOTES

In the following section, we will describe the three YSOs that are previously unknown as eruptive variables. The individual subsections include a description of the photometry and any information that we were able to gather from the literature and that allowed us to include these objects as YSOs displaying long-term outbursts.

A1 V4

V4 (2MASS J02335340 + 6156501) was originally classified as a YSO by Panwar et al. (2014) based on its near-IR excess from 2MASS data. There is no additional literature information for this source. The near-IR JHK_s colours from 2MASS indicate that this is likely a Class II YSO, hence its inclusion in our sample.

The classification as a high-amplitude variable for this source results from its *Gaia* DR2 magnitude being brighter than all of the SSS bands. The object is not visible in the images of the two epochs of *R* band from SSS. Although the SSS catalogues yield a detection with $R = 19.3$ this in fact corresponds to a star located 2 arcsec south west from V4. The variable star becomes visible in the *B* and *I* SSS observations and continues to get brighter as confirmed from the INT photometric Hα survey (IPHAS), Pan-STARRS, and PTF observations (see Fig. B1).

A2 V9

V9 (2MASS J08410676-4052174) is an Hα emission line star (Pettersson & Reipurth 1994), selected from the Marton et al. (2016) catalogue and classified based on its *WISE* colours. This object was selected beacuse its *Gaia* magnitude appeared brighter than expected compared with all of the four SSS bands. Photometry from Vizier confirms this is as a long-term outburst as the object appears to be faint in all SSS epochs with an eruption likely occurring between the second R epoch from SSS and DENIS observations. The object now appears to be slowly declining, as shown by APASS, VPHAS + observations, and the light curve from the Bochum Galactic disc survey (Hackstein et al. 2015). Fig. B2 shows the light curve of V9 as well as the comparison between SSS and VPHAS+ images of the source.

A3 V51

V51 (WRAY 15 − 488) is an Hα emission line star (Wray 1966), which we selected from the Marton et al. (2016) catalogue and classified based on its WISE colours. The object is part of the 139 high-amplitude variable star catalogue as the *R*-band epochs of SSS and *Gaia* DR2 are brighter than the earlier B and I SSS observations. Photometry collected from Vizier confirms its nature as a long-term outburst as the object becomes $\simeq$2.5 mag brighter between 1980 (*I*-band SSS) and 1984 (first epoch in *R* from SSS) and has remained at approximately the same level ever since, as confirmed by data from the All Sky Automated Survey (ASAS, Pojmanski 2002) and SkyMapper (see Fig. B3). Evidence that the object was at a quiescent state when it was classified as an Hα emission line star by Wray (1966) arises from the catalogue of Wackerling (1970) which contains the data from Wray (1966) and where V51 is listed with $V = 13.1$, approximately 3 mag fainter than the current brightness of the object.

This object has spectroscopic observations that confirm its nature as an eruptive YSO. Carmona et al. (2010), based on high-resolution FEROS optical spectra observed in 2004, find that the object shows an Hα P Cygni profile, with an spectrum consistent with that of an F-type giant star. The latter classification is characteristic of eruptive YSOs during outburst (Connelley & Reipurth 2018). Previous spectra, also observed during outburst, from Suárez et al. (2006) and Gregorio-Hetem et al. (1992) are also consistent with an F-type spectral type. V51 also shows broad Na I D 5890Å absorption (Suárez et al. 2006), another characteristic of YSO outbursts, as well as Li I absorption (Gregorio-Hetem et al. 1992), evidence of the youth of the system. Remarkably during these spectra (which are observed at earlier epochs of the outburst than that of Carmona et al. 2010), the Hα line is seen purely in emission.

APPENDIX B: LIGHT CURVES

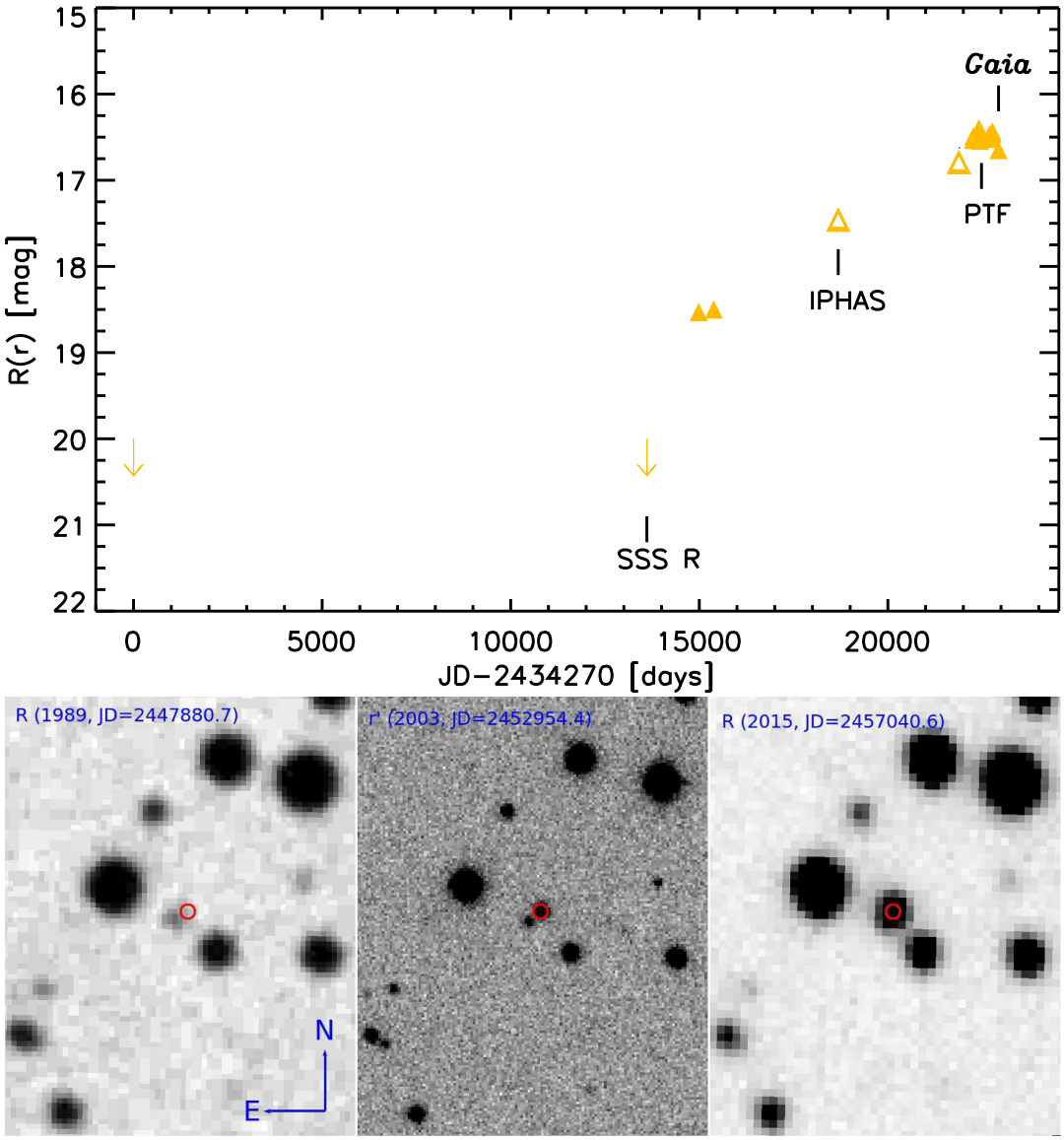

Figure B1. Top: light curve incorporating all available data found in the literature for V4. The photometry from different filters has been converted to approximate *R*-band magnitudes (shown as solid triangles) to help the clarity of the light curve. Sloan *r* filter magnitudes (open triangles) were not converted. In the plot, we mark the approximate epoch of each survey for which we present images in the bottom figure. Bottom: comparison between the *R*-band SSS image obtained in 1989 (left), sloan *r* IPHAS image from 2003 (middle), and the latest PTF *R* image from 2015 (right). In the figure all images have a size of 1 arcmin × 0.8 arcmin.

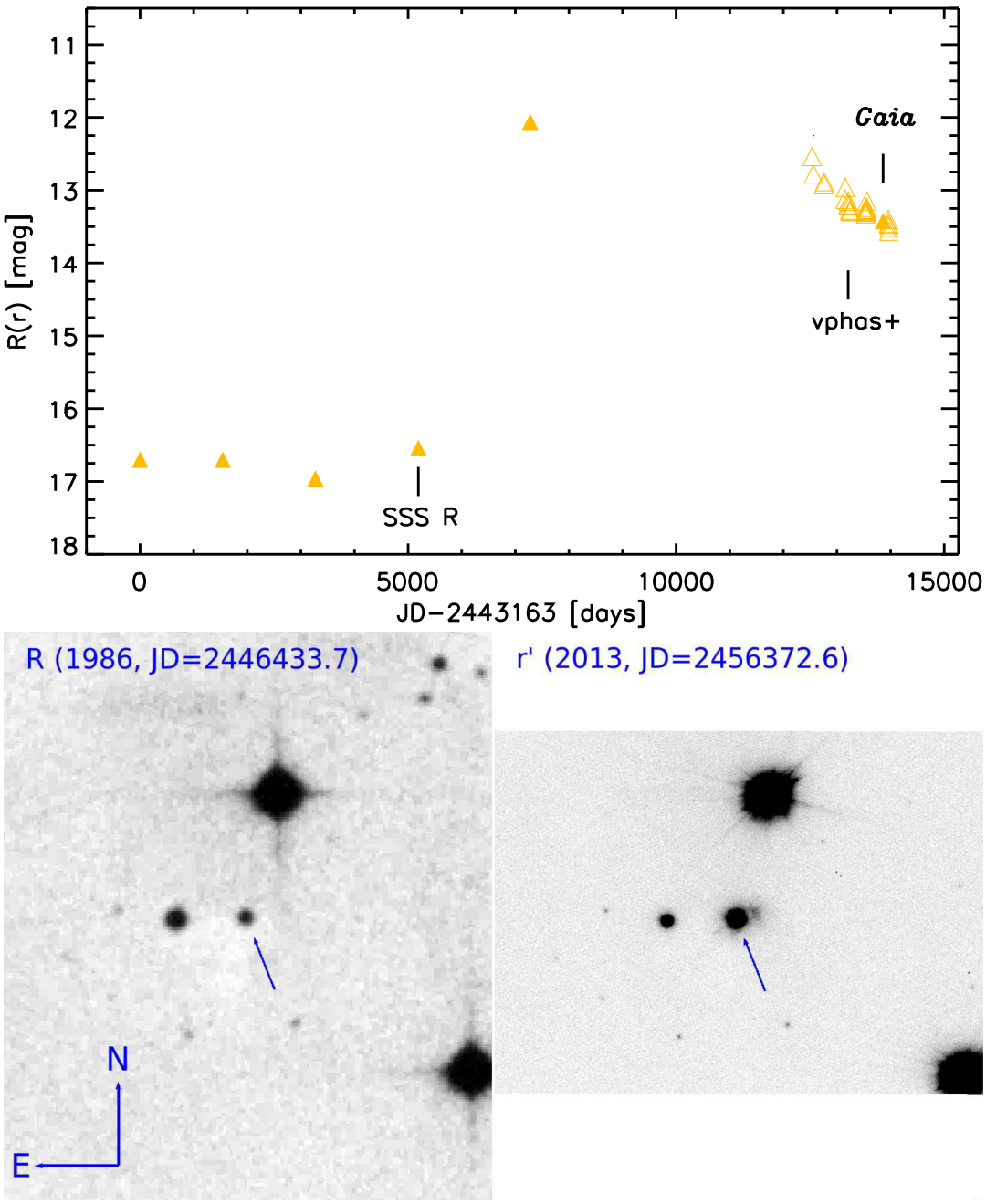

Figure B2. Top: light curve incorporating all available data found in the literature for V9. The photometry from different filters has been converted to approximate *R*-band magnitudes (shown as solid triangles) to help the clarity of the light curve. Sloan *r* filter magnitudes (open triangles) were not converted. In the plot, we mark the approximate epoch of each survey for which we present images in the bottom figure. Bottom: comparison between the second epoch of *R*-band SSS 2.5 arcmin × 2.3 arcmin image obtained in 1986 (left), and the VPHAS+ sloan *r* 1.7 arcmin × 2.3 arcmin image from 2013 (right).

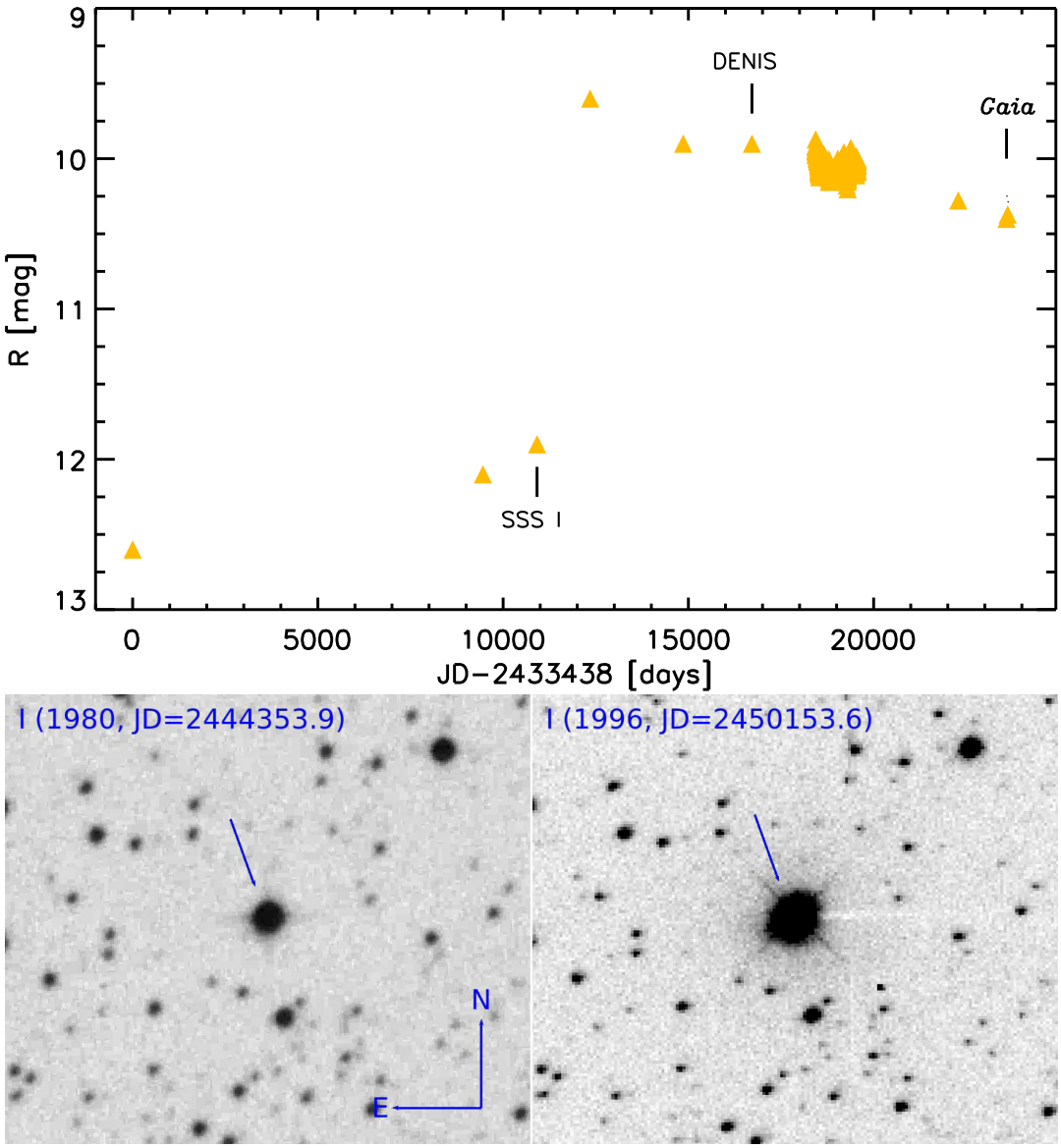

Figure B3. Top: light curve incorporating all available data found in the literature for V51. The photometry from different filters has been converted to approximate *R*-band magnitudes (shown as solid triangles) to help the clarity of the light curve. Sloan *r* filter magnitudes (open triangles) were not converted. In the plot, we mark the approximate epoch of each survey for which we present images in the bottom figure. Bottom: comparison between the *I*-band SSS image obtained in 1980 (left), and the DENIS *I* image from 1996 (right). The images in the figure have a size of 2.5 arcmin × 2.9 arcmin.

APPENDIX C: VIZIER TABLES

This appendix contains the list of surveys used to add photometry to the light curves of our high-amplitude variable YSOs.

Table C1. List of surveys that are part of the analysis of high-amplitude variables found in our study.

Vizier ID	Title	Reference
V/73A/catalog	Third Catalog of Emission-Line Stars of the Orion Population	Herbig & Bell (1988)
III/177/catalog	Observations of Emission-line Stars in the Orion Region I. The Kiso Area A-0904	Wiramihardja et al. (1989)
B/denis/denis	DENIS: A Deep Near-Infrared Survey of the southern sky	Epchtein et al. (1994)
J/AJ/118/1043/tables	A photometric catalog of Herbig Ae/Be stars...UX Orionis stars.	Herbst & Shevchenko (1999)
J/AJ/119/3026/table1	Circumstellar disc candidates identified in the Orion nebula cluster flanking fields.	Rebull et al. (2000)
J/AJ/121/3160/table4	Near-infrared photometric variability of stars toward the Orion A molecular cloud.	Carpenter et al. (2001)
J/AJ/124/1001/table5	Near-infrared photometric variability of stars toward the Chamaeleon I molecular cloud.	Carpenter et al. (2002)
J/AJ/123/387/phot	A photometric study... λ Orionis star-forming region.	Dolan & Mathieu (2002)
J/AJ/123/304/table1	The young cluster IC 5146	Herbig & Dahm (2002)
II/264/var	The All Sky Automated Survey. Catalog of Variable Stars	Pojmanski (2002)
J/AJ/125/1537/table2	Deep near-infrared observations... in Orion Molecular Clouds 2 and 3	Tsujimoto et al. (2003)
J/AN/325/705/table2	Optical and infrared photometry... σ Ori cluster	Béjar, Zapatero Osorio & Rebolo (2004)
J/A + A/417/557/table4	A Rotational and Variability Study of a Large Sample of PMS Stars in NGC 2264	Lamm et al. (2004)
J/AJ/128/2316/table4	The low-mass population of Orion OB1b. I. The σ Ori cluster	Sherry, Walter & Wolk (2004)
J/AJ/128/1684/table1	The initial mass function and young brown dwarf candidates in NGC 2264. I.	Sung, Bessell & Chun (2004)
J/AJ/129/829/table1	The T Tauri star population of the young cluster NGC 2264.	Dahm & Simon (2005)
J/MNRAS/356/89/catalog	Membership, binarity and accretion... σ Ori cluster	Kenyon et al. (2005)
II/271A/patch2	TASS Mark IV Photometric Survey of the Northern Sky	Droege et al. (2006)
2mass-psc	2MASS All-Sky Catalog of Point Sources	Skrutskie et al. (2006)
J/ApJ/662/1067/sigori	A *Spitzer Space Telescope* study of disks in the young σ Ori cluster	Hernández et al. (2007)
J/MNRAS/375/1220/ngc2264	Empirical isochrones and relative ages for young stars... NGC 2264	Mayne et al. (2007)
J/MNRAS/375/1220/sigori	Empirical isochrones and relative ages for young stars... σ Ori	Mayne et al. (2007)
II/319/gcs9	UKIRT Infrared Deep Sky Survey (UKIDSS) Release 9	Lawrence et al. (2007)
II/316/gps6	UKIRT Infrared Deep Sky Survey (UKIDSS) Galactic Plane Survey (GPS) Release 6	Lucas et al. (2008)
J/ApJS/183/261/table2	A multicolour optical survey of the Orion nebula cluster. I. The catalog.	Da Rio et al. (2009)
J/ApJS/191/389/table2	Precision photometric monitoring of very low mass σ Orionis cluster members	Cody & Hillenbrand (2010)
J/ApJ/726/18/stars	Disk evolution in W5: intermediate-mass stars at 2–5 Myr	Koenig & Allen (2011)
J/ApJ/733/50/table2	YSOVAR: ... mid-IR photometric monitoring of the ONC	Morales-Calderón et al. (2011)
J/A + A/525/A47/tablec2	U-band study of the accretion properties in the σ Ori star-forming region	Rigliaco et al. (2011)
J/AZh/88/143/oricat	Proper motions of stars in the region of the Great Nebula in Orion	Vereshchagin & Chupina (2011)
J/A + A/548/A79/omc-var	INTEGRAL-OMC optically variable sources	Alfonso-Garzón et al. (2012)
J/ApJ/751/22/table3	A significant population of candidate new members of the ρ Ophiuchi cluster	Barsony et al. (2012)
J/ApJ/752/59/members	The low-mass stellar population in L1641...stellar initial mass function	Hsu et al. (2012)
II/313/table3	The Palomar Transient Factory photometric catalogue 1.0	Ofek et al. (2012)
J/ApJ/754/30/youth	New isolated planetary-mass objects...σ Orionis cluster.	Peña Ramírez et al. (2012)
J/MNRAS/434/806/catalog	Pre-main-sequence isochrones. II. Revising star and planet formation time-scales.	Bell et al. (2013)
J/ApJS/209/28/table2	The MYStIX wide-field near-infrared data: optimal photometry in crowded fields	King et al. (2013)
II/321/iphas2	The Second Data Release of the INT Photometric H-Alpha Survey...	Barentsen et al. (2014)
J/A + A/564/A29/catalog	Orion Revisited: II. The foreground population to Orion A	Bouy et al. (2014)
II/341/vphasp	The VST Photometric Halpha Survey... (VPHAS +) DR2.	Drew et al. (2014)
J/ApJ/794/36/table2	A spectroscopic census in young stellar regions: the σ Orionis cluster.	Hernández et al. (2014)
J/other/RAA/14.1264/table1	V350 Cep UBVRI long-term photometry	Ibryamov, Semkov & Peneva (2014)
I/327/cmc15	The Carlsberg Meridian Catalogue, final data release (MC15)	Muiños & Evans (2014)
V/147/sdss12	The SDSS Photometric Catalogue, Data Release 12 (DR12)	Alam et al. (2015)
J/AJ/149/200/table4	An optical survey of the partially embedded young cluster in NGC 7129	Dahm & Hillenbrand (2015)
II/336/apass9	AAVSO Photometric All Sky Survey (APASS) DR9	Henden et al. (2015)
J/ApJS/220/17/table2	Wide-field infrared polarimetry of the ρ Ophiuchi cloud core	Kwon et al. (2015)
J/AJ/150/132/variables	Near-infrared variability in the Orion Nebula Cluster	Rice et al. (2015)
J/A + A/581/A140/tablea2	The VISTA Orion mini-survey: star formation in the Lynds 1630 North cloud.	Spezzi et al. (2015)
II/349/ps1	Pan-STARRS DR1	Chambers et al. (2016)
J/A + A/587/A153/science	VISION - Vienna survey in Orion. I. VISTA Orion A Survey.	Meingast et al. (2016)
II/348/vvv2	VISTA Variable in the Via Lactea Survey DR2	Minniti et al. (2017)
Not in Vizier	Northen Sky Variability Survey (NSVS)	Woźniak et al. (2004)
Not in Vizier	The Catalina Real-Time Transient Survey (CRTS)	Djorgovski et al. (2011)
Not in Vizier	Pan-STARRS DR2	Chambers et al. (2016)
Not in Vizier	The HOYS-CAPS Citizen Science Project	Froebrich et al. (2018)
Not in Vizier	The American Association of Variable Stars Observers (AAVSO)	Kafka et al. (2018)
Not in Vizier	SkyMapper Southern Sky Survey	Wolf et al. (2018)

This paper has been typeset from a TEX/LATEX file prepared by the author.